Study of Phases of Matter: Dipolar Dimer Liquid and Topological Metamaterials with Odd Elasticity

Junyi Zhang

A Dissertation
Presented to the Faculty
of Princeton University
in Candidacy for the Degree
of Doctor of Philosophy

Recommended for Acceptance
by the Department of Physics
Adviser: Prof. F. D. M. Haldane

September 2021

Abstract

Phases of matter are splendid, and get more complicated from physical systems to biochemical systems. Simple physics principles are proposed to categorise various phases of matter. The physical principles are often exemplified by simple idealised models. When they are applied to more complicated biochemical systems, some generalisations may be needed.

In this thesis, two idealised models, dipolar dimer liquid and topological metamaterials with odd elasticity, are discussed. The first model, Dipolar Dimer Liquid (DDL), is motivated by water. It is a simplified model consisting of dipolar dimers on lattice with a Coulombic interaction between the dimers. The Coulombic interaction is an idealised model for the hydrogen-bond interaction. It is found that there exists a liquid-liquid phase transition in this model. To understand this phase transition, an exact mapping from the DDL to the annealed Ising model on random graphs has been constructed. Consequently, one may identify the order parameter charactering the liquid-liquid phase transition of the DDL with the order parameter of the Ising model, magnetisation. One may further bound the critical temperature with the help of this exact mapping and the exactly solved Ising models in 2D. The estimation of the critical temperature has been confirmed by the numerical simulations. A quantum generalisation of the DDL has also been proposed. Interesting interplay of the Coulombic interaction and the quantum solid-liquid transition is discussed.

The second model is motivated by active matter. In the presence of active energy pumping, a strange stress response, the odd elasticity, is admissible. In our model, the odd elasticity comes from an idealised model of metabeams, and the dynamics of the system becomes non-Hermitian. Interestingly, the topological properties still survive in the non-Hermitian dynamics. But the bulk modes also become exponentially localised, which is called non-Hermitian skin effect. To characterise the topological properties, the definition of the Brillouin zone has been generalised, and the definition of the Zak-Berry phase has been clarified for the non-Hermitian systems. The 1D rotor chain and 2D rotor lattice have been discussed in detail as demonstrating examples.

To my parents.

Acknowledgements

Figure 1: Portrait of Richard Feynman by Jiachen Li for my birthday present. I appreciate Feynman's philosophy of pedagogy, and make my best to practise it.

I would first acknowledge Prof. Haldane's advising over the years of my PhD study. Prof. Haldane shared with me his distinguishing insights into various physical problems. Sometimes it is very challenging to get an idea in the beginning, but once tunneling through the barrier, I am always amazed by the kingdom he guides me to.

I would also acknowledge Prof. Lieb for his encouraging and helpful discussions. After I finished my first draft of the article on DDL, I happen to find that Prof. Lieb appeared almost in every reference either as an author or in the acknowledgement. Prof. Lieb's works over the last three score years provide endless bricks for my building of the castle. He is always energetic and propels me going ahead.

I collaborated with Dr. T. Neupert at the beginning of my PhD study when he was postdoctoral fellow at PCTS. Discussions with Titus made up the gap of my knowledge from the textbooks and that in the frontiers of the research. The second project on non-Hermitian topological metamaterials in this thesis was in collaboration with Dr. D. Zhou. Di attracts me to the soft regime of the condensed matter physics, where the ideas I learnt in a quite different context may have some

unexpected applications and generalisations.

I would also thank Prof. Huse for the discussions with him. It is often helpful because he always hits the key point, but sometimes it is also "discouraging" because he probably had worked out the same problem decades ago. Prof. A. M. Polyakov's course on modern classical dynamics is one of my favourite courses. Alexander Markovich merged his deep thoughts into simple examples of classical mechanics, and he opened for me a window towards the hydrodynamics and turbulence. Sometimes, I may not be able to appreciated the full elegance of Alexander Markovich's point of view until I encounter an application in my research project. Some of my research projects with Prof. Haldane was motivated by the experiments conducted in Prof. Ong's group. Prof. Ong is always a correct person to resort to for clarifying what I do not understand in a discussion with Prof. Haldane. Prof. Sondhi motivated me on the generalisation of the DDL to quantum regime. He also motivated me to think more about quantum information.

I also organised a discussion group on various topics in maths, natural sciences and engineerings. I would acknowledge the contributions from all the participants, without whom it would be impossible. Due to the COVID19, we moved online, which, nevertheless, encouraged more discussions with friends at distance.

I would thank Prof. Nozomi Ando and Prof. Nieng Yan, from whom I learnt about biochemistry. I would thank Prof. William Phillips, Prof. Gretchen Campbell and the group members, with whom I did my experimental project on building a laser for Sr. I would thank Dr. Hao Zheng, in collaboration with whom I learnt about quantum dots and have an article published on double quantum dots.

I would also thank Yu Shen, Jie Wang, Ilya Belopolski, Zijia Cheng, Jun Su, Antoine Song, Mansour Shayegan, Michael Zaletel, Xi Lin, Pengjie Wang, Wudi Wang, Biao Lian, Ziming Ji, Ruixing Zhang, Yunqin Zheng, Huan He, Yayun Hu, Jennifer Cano, Nicholas Quirk, Zheng Ma, Xiaowen Chen, Nana Shumiya, Fang Xie, Bogdan Andrei Bernevig, Kasey Wagoner, Peter Meyers, Athanassios Panagiotopoulos, Silke Biermann, Boyu Zhang, Guang Chen, Chong Sun, Lizao Ye, Leticia Cugliandolo, Norman Jarosik, Jiachen Li, Jiayi Hu, Jieru Shan, Hongwu Qian, Xiao Fan, Yimo Han, Yichen Fu, Jiaqi Jiang, Ming Lyu, Haina Wang, Bin Xu, Catherine Brosowsky, Anya Bartelmann, Conan Edogawa, ... It is impossible to have a complete list of all people I would thank for the helps and the encouragement.

Contents

Chapter 1

Introduction

One of the central tasks of the condensed matter physics is to understand various phases of matters. It is now often referred to as Landau's paradigm of phase transition, where different phases are distinguished by their symmetries. A phase with higher symmetry is often less ordered. For example, in a liquid state, atoms do not have fixed distance between each other. Then, after thermal averaging, the liquid phase has continuous translational and rotational symmetries. While in a solid state, atoms are arranged according to some crystalline pattern at fixed positions, Therefore, the solid phase has only discrete crystal symmetries. In the solid-liquid phase transition, when the solid melts, it restores the translational and rotational symmetries, and reversely when the liquid solidifies, the symmetries are spontaneously broken. In order to characterise the phases in a more quantitative manner, Landau introduced *order parameter*, then the free energy of the system can be written as a functional of the order parameter [42]. This paradigm turns out to be quite successful, as it applies to a wide variety of phase transitions, e.g., solid-liquid transitions, magnetic transitions, superconductivity, etc.

In thermodynamics, the free energy F of a system contains of two terms often playing competing rôles, the energy E and the entropy S. The free energy F and the energy E are related by the Legendre transformation

$$F = E - TS, \tag{1.1}$$

where T is the temperature. The entropy measures the disorderedness of a system. At higher temperature, the second term weighs more, so the system tends to be less ordered. In the solid-liquid phase transition, there is often a latent heat, therefore the entropy of the system changes discontinuously. This kind of phase transition is called first-order transition. On the contrary, in the

superconducting-normal transition in zero magnetic field, the entropy changes continuously, but its derivative (e.g., the heat capacity) has a jump. This kind of phase transition is called second-order transition.

In the second case, Landau assumed that the dependence of the free energy on the order parameter near the critical temperature T_c has the form

$$F_{\text{pot}} = \int (\mathrm{d}^D x) \left(\frac{1}{2}\alpha(T)(\phi)^2 + \frac{1}{4}\beta(\phi)^4 \right), \tag{1.2}$$

where D is the spatial dimension, $\alpha = a_0(T - T_c)$ changes sign at T_c, and a_0 and β are positive constants. The order parameter may also fluctuate in the space. Therefore, there is also a term depending on the gradient of the order parameter $\nabla\phi$ in the free energy functional, i.e.,

$$F_{\text{grad}} = \int (\mathrm{d}^D x) \frac{1}{2} K(\nabla\phi)^2, \tag{1.3}$$

where K quantifies the stiffness of the order paramter.

If the fluctuations are strong, the long-range order can be destroyed. It is now known as a seminal theorem named after Mermin, Wagner, and Hohenberg [1] that a continuous symmetry will not spontaneously break in systems of dimension $D \leq 2$ and with short-range interaction. This is a consequence of the divergent correlation of the Goldstone mode in the infrared (IR) limit.

In quantum systems, the fluctuations may originate from the quantum effects, e.g., the zero-point energy in liquid Helium. A phase transition can be achieved by tuning the parameters of the system even in the limit of $T \to 0$, which is often referred to as quantum phase transition, and the point in the parameter space separating two phases is called quantum critical point. In 2D antiferromagnetic Heisenberg model, if one adds a strong enough easy-axis anisotropy, the system will be ordered. Such an ordered phase is in the universality class of Ising model in the sense of renormalisation group.

In 1970s, people realised that there are phase transitions beyond Landau's paradigm [8, 9, 39]. For instance, in 2D XY model, since there is a continuous in-plane rotational symmetry, there should be no long-range ordered phase according to the Mermin-Wagner-Hohenberg theorem. However, Berezinskii [8, 9] and Kosterlitz and Thouless [39] respectively noticed that there is a critical temperature T_{BKT} above which there is a significant contribution to the fluctuations due to the

[1] Sometimes the name list also includes Berezinskii and Coleman.

vortices. In Ref. [39], one estimated the free energy for a vortex according to Eq. 1.1,

$$F_v = \frac{1}{2}q^2 \ln(R/a_0) - k_B T \ln(R/a_0), \tag{1.4}$$

where q denotes the vortex charge, R is the size of the system, and a_0 is size of the vortex core. The first term is the excitation energy of a vortex, and the second term is proportional to its configurational entropy. Then, the critical temperature T_{BKT} can be estimated as the second term starts to dominate, i.e., $k_B T_{\mathrm{BKT}} \sim \frac{1}{2}q^2$. In either case, above or below T_{BKT}, there is no long-range order in the sense of the order parameter ϕ. But the correlation function $\langle \cos\phi(x_1)\cos\phi(x_2)\rangle$ is decaying algebraically below T_{BKT}, which is a reminiscent of the long-range order. Below T_{BKT}, the phonon-like fluctuations destroy the long-range orders, but above the T_{BKT}, vortex pairs are free to be created and to proliferate. The excitations of the vortices are topological objects. Therefore, this kind of phase transitions is also called topological phase transition.

Phases of a system bearing topological low-energy excitations or phases themselves characterised by some topological invariants are called topological phases. Topological phases often have some properties robust against the perturbations. In quantum systems, the robust properties can be ground state degeneracy, topologically protected edge states, etc. One of the earliest examples was pointed out by Haldane [20] that spin-1 antiferromagnetic Heisenberg chain is gapped and it supports topologically protected spin-$\frac{1}{2}$ excitations at the boundaries [2]. This feature of the topological phases is often called *bulk-edge correspondence*.

The discovery of the quantum Hall effects, integral [37] and fractional [79], turns out to be a milestone. Over the last three decades, the development of the theory of topological phases of matters branched into two major categories; however both of them can be dated back to the quantum Hall effects as prototype. The precise quantisation of the Integer Quantum Hall Effect (IQHE) has been attributed to the topological nature of the Hall conductance [77]

$$\sigma_H = \frac{e^2}{h}C, \tag{1.5}$$

where C is an integer called Chern number and $\sigma_0 = \frac{e^2}{h}$ is the conductance quantum. (The inverse of the conductance quantum $R_K = \sigma_0^{-1}$ is also known as von Klitzing constant.) On the boundaries, the Landau levels are bended upwards by the confining potential and form the conducting chiral edge states [23]. A simple but insightful model of IQHE without Landau level was constructed by Haldane [21], where the Chern number C is equal to the integral of the Berry curvature over the

Brillouin zone. There also exist C branches of chiral edge states. Haldane's idea was not well appreciated until around 2005, when the quantum spin Hall effect was proposed theoretically [55, 32] and soon realised experimentally [38], where the edges consist of pairs of helical states. The 3D correspondence of the quantum spin Hall effect is called topological insulator, i.e., the bulk being gapped insulator but the surfaces being metallic due to the topologically protected gapless Dirac cones. On the other hand, the emergence of the fractionally charged excitations in the Fractional Quantum Hall Effect (FQHE) cannot be understood without interactions. Its topological nature is revealed by its edge excitations described by the chiral Luttinger liquid [82]. Exotic fractional excitations are not only of theoretical importance [81], they may also serve as candidates for topological quantum computation [36].

The concept of classification of phases with symmetry and topology applies not only to the solid state matters, it may also apply to many other systems that appear quite different. Extensions may be needed to accommodate new features. Here, we mention two examples that will be heuristic to the development of the models discussed in Chap. 2 and Chap. 3.

Let us first consider the classical fluid. The classical fluid is described by the Navier-Stokes equation

$$\partial_t(\rho u^i) + \partial_j(\rho u^i u^j) = -\delta^{ij}\partial_j p + \partial_j(\mu \mathcal{S}[\delta^{jk}\partial_k u^i]) + f^i, \tag{1.6}$$

where ρ is the (mass) density of the fluid, $\mathbf{u} = (u^i)$ is the velocity field, p is the mechanical pressure, μ is the coefficient of viscosity, and $\mathbf{f} = (f^i)$ is the body force density [44, 59, 18, 74]. The symbol $\mathcal{S}[T^{ji}]$ means the symmetric traceless part of the tensor T^{ji}. This equation is nothing but Newton's equations of motion applied to macroscopically small and microscopically large fluid particles. We have further equations of continuity and incompressibility

$$\begin{aligned} \partial_t(\rho) + \partial_j(\rho u^j) =& 0, \\ \partial_j(u^j) =& 0. \end{aligned} \tag{1.7}$$

By homogeneity of the water, we also assume the fluid has a constant density ρ. Then, the Navier-Stokes equation can be written in a form more commonly cited as

$$\partial_t(u^i) + u^j\partial_j(u^i) = -\delta^{ij}\partial_j\tilde{p} + \eta\Delta u^i, \tag{1.8}$$

where $\tilde{p} = \frac{p}{\rho}$ is the reduced pressure, $\eta = \frac{\mu}{\rho}$ is often referred to as kinematic viscosity, Δ is the Laplacian, and we have omitted the term of body force. By abuse of language, we will omit the tilde for the reduced pressure and also call it pressure, which should be clear from the context without ambiguity. In the incompressible flow, the pressure may be regarded as a Lagrange multiplier for the constraint of volume conservation.

The Navier-Stokes equation is notorious for its non-linearity in the convection term (second term on the left hand side of Eq. 1.8). Therefore, the generic existence of the solutions to the Navier-Stokes equation is still an open problem in mathematics. However, it is also due to this nonlinear term, various intriguing phenomena arise, particularly the turbulence. Although, rigorous mathematical study of turbulence turns out to be extremely hard, there are some heuristic physical methods developed for the turbulent systems. For example, the high frequency fluctuations of the physical quantities can be taken statistically [52]. This point of view turns out to be fruitful, e.g., in understanding the scaling behaviour in turbulent flows in analogy to the critical phenomena in statistical physics [19]. This example is for demonstrating the application of the concepts of statistical physics to systems appearing quite different. In this thesis, I will not pursue further in the theory of turbulence.

The stress response in Eq. 1.6 is not in its most general form. In the quantum Hall fluid, the antisymmetric part of the viscosity tensor may also contribute to the stress tensor, which is called Hall viscosity [7]. The Hall viscosity does not dissipate energy, and it is of quantum nature [62, 63, 60]. The non-vanishing Hall viscosity is only possible when the time reversal symmetry is broken. There is an exact analogy in solid system, where an odd elasticity may contribute to the stress tensor [67]. In contrast to the Hall viscosity, the odd elasticity does not conserve the energy. Therefore, it leads to non-Hermitian dynamics . Odd elasticity does not appear in ordinary electronic systems, while it may naturally arise in active matters, which will be discussed in Chap. 3.

The second example is the collective motion of flocks of fishes or birds. The motion is described by a velocity field $\mathbf{v}(\mathbf{r})$. It is intuitive to make an analogy between the ferromagnetic phase to the flocks collectively moving with a non-vanishing mean velocity. One may assume that a bird may follow other birds in its sight even if those ones are at a far distance. Therefore, if one would like to build an effective model based on spins $\mathbf{s} = \mathbf{v}/|\mathbf{v}|$, there will be non-local interactions [10]. In microscopic systems of electrons, there is no mechanism of couplings as such from the first principle. In an effective model, nothing forbids such interactions to arise [72]. A more sophisticated model describing the motions of the flocks was due to Vicsek *et al.* [80], which is often referred to as Vicsek model. In this model, one regards the positions of the birds as dynamic variables in addition to

the velocities. Although one assumes that a bird only watches other birds within a finite range, an effective non-local interaction can still arise, because the neighbours of a bird keep varying during the period of flying. These two points of view of the flocks bear ideas similar to Euler's view of a fisherman versus Lagrange's view of a fish in hydrodynamics [59]. It turns out that biological systems consisting of self-propelling particles as in Vicsek model may behave in a way quite different from the classical fluids. The resulting phases may belong to new universality classes.

In this thesis, I studied two systems with motivations from some chemical and biological systems. Chemical and biological systems provide intriguing test fields for physical theories. Although the fundamental equations of motion are governed by the Schrödinger or Dirac equation, it is hard to solve the equations if not impossible. Nevertheless, as various scales emerge, new effective theories may be needed to reveal the underlying physics.

The first system is motivated by the hydrogen-bond interaction in water. It is known that the hydrogen-bond interaction is indispensable in understanding some peculiar properties of water, e.g., the hydrophobic effect and the anomalous thermal expansion, etc., as well as in many biochemical processes, e.g., the protein folding problem. In the former case, Molecular Dynamics (MD) simulations provided some evidence how the water molecules are organised in the presence of the hydrogen-bond interaction. In the latter case, in spite of the huge progress achieved recently base on deep learning method [70, 16], the underlying physical picture still lacks. Instead of tracking every detail of the complicated systems, hopefully studying idealised model may help to reveal the underlying physics more effectively. I proposed a lattice liquid model of dipolar dimers with Coulombic interactions which is named Dipolar Dimer Liquid (DDL). I showed that it has an interesting phase where the dipolar dimers are ordered by the Coulombic interaction but without breaking the translational symmetry or the rotational symmetry. Recently, MD simulations of realistic models of water indicate a second critical point in supercooled water [14]. It seems the result of the MD simulations echoes the phase transition I found in DDL in various aspects. Furthermore, I studied its quantum generalisation. In contrast to the classical DDL, the Coulombic interaction does help to stabilise the solid phase in quantum DDL.

The second system reported in this thesis is motivated by active matters. In superconductors, when an external magnetic field is applied to it, a current will form so as to screen the magnetic field. This screening is possible only if the current is dissipationless. Unlike the electrons in solids, active matters may consist of self-propelling particles as exemplified in the Vicsek model. In active matter, as the particles are able to propel themselves, there may be a spontaneous current, which naturally breaks the time reversal symmetry. If the arrangement of the current is chiral, one obtains

an analogue of quantum Hall effect in active liquid [73]. It should be noticed that the spontaneous current in active liquid also violates the conservation law of the energy, while this is not surprising as the active particles eat and convert the chemical energy to kinetic energy. Therefore, the dynamics of the active matter may well be non-Hermitian. Bearing this in mind, in collaboration with Di Zhou, we studied a model of active matter with *odd elasticity*. The concept of the topological state can still be defined in this system even if it is governed by the non-Hermitian dynamics. In contrast to the Hermitian electron systems, the bulk states may also be localised, which is called non-Hermitian skin effect [41, 86]. We also clarified the proper generalisation of the Zak-Berry phase for the non-Hermitian systems [71], which may still be used to indicate the existence of the topological modes.

Chapter 2

Dipolar Dimer Liquid: Water and Beyond

In this chapter, the model dipolar dimer liquid will be discussed. We first briefly review some basic aspects about the water molecule that one learnt from *ab initio* calculations, and the knowledge about liquid and solid phases of water from MD simulations. One of the very successful models accounting for the residual entropy in ice was pioneered by Pauling [58]. Lieb considered a more idealised model than Pauling's, i.e., a 2D square ice that is also known as the six-vertex model, and solved it exactly [47]. In Ref. [47], the residual entropy density of the 2D square ice is obtained by the transfer matrix method, and the constant $W = \left(\frac{4}{3}\right)^{3/2}$ is now often referred to as Lieb's constant. Motivated by Pauling's and Lieb's thoughts, I proposed a new idealised lattice liquid model, DDL. In the DDL, molecules are represented by dipolar dimers, and they are free to move. Therefore, DDL describes a liquid phase. More importantly, the hydrogen-bond interaction is also taken into account by considering a Coulombic interaction between the dipolar dimers. The precise definition is given in Sec. 2.1

In Sec. 2.2, it is shown show that there exists a liquid-liquid phase transition in the DDL. In the ordered phase, no translational or rotational symmetries of the dimer is broken. In fact, the spatial charge distribution is ordered by the Coulombic interaction. This phase looks very similar to the ice, but it is NOT ice because the molecules (dimers) do not form a crystal. Furthermore, the partition function of the system looks like that of a glassy system. Therefore, I named this phase *glacia* phase. [1] With an involved construction, the DDL can be mapped exactly to the annealed Ising model on

[1] The word *glacia* is the Latin word for ice, and it sounds like glass. This name shall remind people of an ice-like phase with a glass-like partition function.

random graphs. Resorting to the knowledge of the Ising models (particularly in 2D), one is able to bound the glacia phase transition of the DDL on 2D lattice quite tightly. It should be emphasised that the exact mapping constructed in Sec. 2.2 is independent of the dimension. Therefore, we believe that the glacia phase transition in 3D should also be described by the universality class of 3D Ising model, which seems to be consistent with a recent report of MD simulations of the supercooled water [14].

In Sec. 2.3, the Monte Carlo (MC) simulation of the DDL is discussed. The sampling method is not trivial. When dimers completely covered the lattice, the usual sampling scheme based on local dimer motions does not work because it cannot run through all possible states. By resorting to Lieb's representation of the dimer model [48], the DDL is mapped to two coupled Ising models, which legitimates the sampling strategy for the MC simulation. The numerical result confirms our prediction without surprise.

In Sec. 2.4, a generalisation to quantum DDL is described. One observes that, although the Coulombic interaction does not solidify the DDL, it does help to stabilise the solid phase in quantum DDL. The Rokhsar-Kivelson point is shifted by the Coulombic interaction, and the critical point for the quantum solid-liquid transition of the quantum DDL is estimated.

2.1 Modeling the Water

A water molecule consists of one oxygen atom and two hydrogen atoms. The oxygen atom has its orbitals sp^3-hybridised and two of the hybridised orbitals form covalent bonds with the hydrogen atoms by sharing a pair of electrons for each bond. Two other hybridised orbitals are occupied by the lone pairs of electrons. Since the lone pairs are not shared with other hydrogen atoms, they are closer to the core of the oxygen atom, and they make the HOH-bond angle slightly smaller than that of a tetrahedron ($2\arctan\sqrt{2} \approx 109.5^\circ$). The oxygen site is therefore negatively charged and the hydrogen sites are positively charged. The OH-bond energy is of the order of several eV. This picture has been essentially confirmed by *ab initio* calculations.

If there are two water molecules, they will interact with each other. When they are far apart, each of the water molecule may be regarded as an electric dipole. This dipole-dipole interaction is described by

$$H_{I,DD} = -\frac{1}{4\pi\epsilon_0}\frac{3(\mathbf{p}_1\cdot\hat{\mathbf{r}})(\mathbf{p}_2\cdot\hat{\mathbf{r}}) - \mathbf{p}_1\cdot\mathbf{p}_2}{r^3}, \tag{2.1}$$

where ϵ_0 is the vacuum permittivity, $\mathbf{r}$ is the position vector pointing from one dipole to the other,

r is the length of $\mathbf{r}$ and $\hat{\mathbf{r}} = \frac{\mathbf{r}}{r}$ is the unit vector in the direction of $\mathbf{r}$.

At Standard Temperature and Pressure (STP) [2], the distance between two ideal gas molecule is about 3nm. The dipole moment of the water molecule is about $p_w \approx 6 \times 10^{-30}\mathrm{C} \cdot \mathrm{m}$. By Eq. 2.1 we may estimate the typical energy scale of the dipole-dipole interaction $E_{g,DD} \approx 0.08\mathrm{meV}$ for two water molecules in gas phase, which is much smaller than the typical energy scale of the kinetic energy $E_K = \frac{3}{2}k_BT \approx 40\mathrm{meV}$. When the water molecules are in liquid phase, the typical distance between the molecule is only one tenth of that in gas phase, so the dipole-dipole interaction can be a thousand times stronger, i.e., $E_{l,DD} \approx 80\mathrm{meV}$, which is comparable to E_K.

Furthermore, the distance between the molecules in liquid phase is comparable to the size of the molecule. Therefore, Eq. 2.1 is no longer a good approximation. If we assume the polar charge distribution is pointwise localised on the atoms, then the total interaction energy should be calculated according to Coulomb's law by summing up pairwise Coulomb interactions

$$H_{I,C} = \sum_{(i,j)} \frac{1}{4\pi\epsilon_r\epsilon_0} \frac{q_i q_j}{r_{ij}}, \tag{2.2}$$

where q_i is the charge carried by atom i and r_{ij} is the distance between atom i and atom j. The relative permittivity ϵ_r is a mean field approximation of the other molecules as a homogeneous medium.

In addition to the Coulomb interaction, there are also van der Waals interaction between the molecules, which is attractive and is proportional to r^{-6}. However, when two molecules are very close together, the interaction become repulsive. One of the empirical potentials often used in MD simulations is the Lennard-Jones potential

$$H_{I,L-J} = 4\epsilon \left[\left(\frac{\sigma}{r}\right)^{12} - \left(\frac{\sigma}{r}\right)^{6} \right], \tag{2.3}$$

where the minimum of the potential is at $r_m = 2^{1/6}\sigma$ and the corresponding potential energy is $V_{eq} = -\epsilon$.

The interactions in Eq. 2.2 and Eq. 2.3 has been implemented for MD simulations with semi-empirical parameters. For example, in a model named TIP3P, a water molecule consists of three rigidly connected atoms (sites) with charges and Lennard-Jones parameters specified for the atoms. An improved model widely used in MD simulations for water is TIP4P where a fictitious M site (often massless, where the charge of the oxygen is placed) is added compared to the TIP3P model. There

[2] Defined by IUPAC, the temperature is $273.15K = 0°\mathrm{C}$ and the pressure is $1 \times 10^5\mathrm{Pa}$. The molar volume of the ideal gas at STP is $0.0227\mathrm{m}^3$.

are variants of TIP4P model with slightly different parameters, e.g., TIP4P/2005 and TIP4P/Ice that are often regarded as quite good classical force fields for water in the sense of their ability to reproduce the stability of various ice phases [1].

Among the complicated interactions between the molecules, it is the hydrogen-bond interaction that makes water particularly interesting. It is more than the simple Coulomb interactions due to the partial charges carried by the atoms. From the perspective of quantum chemistry, the hydrogen atom in one water molecule (covalently bonded with the oxygen atom in the molecule) is interacting with the oxygen atom in another water molecule by overlapping its antibonding orbital with the lone pair orbital. Therefore, the covalent OH-bond is weakened by the hydrogen-bond interaction whereas the hydrogen bond looks partially like a covalent bond in contrast to the Coulomb and the van der Waals inter-molecule interactions. A typical strength of the hydrogen bond in water is estimated to be about 200meV. So it is important to handle the hydrogen bond properly so as to understand various effects in water, e.g., the formation of various phases of ice.

The problems in biological systems are more complicated. The hydrogen-bond interaction does not only exist in water, it is ubiquitous in biological molecules and is essential for the structures of DNA, RNA and protein. The good models for pure water, like the ones mentioned above, might not be good enough in the presence of these biological molecules. After all, in the spirit of Dirac, all the atoms and the electrons should obey the same "Schrödinger" equation on the very basic level. There do be recent progress on implementing MD simulations more "fundamentally" than with these semi-empirical force field models, where the interactions are computed with *ab initio* methods or Density Functional Theory (DFT) [91]. I will not pursue further details of various approximation schemes used in MD simulations. Perspective of MD simulation will be discussed in Sec. 2.5.

An alternative philosophical parcours in contrast to the reductionism is the emergence theory that has been advocated by one of the pioneers of the condensed matter physics, Philip Anderson [6]. A milestone in this spirit is the universality and the renormalisation theory of the critical phenomena. For instance, the magnetisation, superconductivity and liquid-gas phase transition can all be described by the same physics law. In this sense, we *understand* the physics beyond splendid emergent phenomena. Bearing this in mind, I will propose a simplified model for water. Although the model may appear crude, hopefully it captures some key ingredients of the problem, and will help us to understand the physics.

An early example may be dated back to Yang and Lee's discussion on liquid-gas phase transition [85, 46]. Yang and Lee studied liquid-gas phase transition of molecules with Lennard-Jones like interactions, i.e., a short range attractive interaction with a hard core repulsion [85]. The key

features of this phase transition are quite well captured by a much more simplified model, i.e., the lattice gas model [46]. They mapped the lattice gas model to the Ising model, while the later has been exactly solved. It is heuristic to describe their model in more details. Suppose there is a lattice and each lattice site can be occupied by an atom or left vacant. Two atoms are not allowed to occupy the same site due to the hard-core repulsion. If two atoms sit on neighbouring sites of the lattice, they attract each other with an energy $u = -2\epsilon$; if they are far part, then they do not interaction with each other, or $u = 0$. So the Hamiltonian of this lattice gas is

$$H_{G,LY} = -2\epsilon N_{\rm nn}, \tag{2.4}$$

where $N_{\rm nn}$ is number of pairs occupying nearest neighbour sites. The rule of mapping this lattice gas model to the Ising model is as follows. On each lattice site one put a spin, either pointing up or down. If a spin is pointing down, it means this site is occupied by an atom; otherwise the site is vacant. The Hamiltonian can be transcribed in terms of the Ising model as

$$H_{I,LY} = -J \sum_{\langle i,j \rangle} S_i S_j + h(N_\downarrow - N_\uparrow), \tag{2.5}$$

where S_i is the spin on site i and N_S is the number of spins in state S. Therefore, $N_{\rm nn} = N_{(\downarrow\downarrow)}$, i.e., number of neighbouring pairs with both spin down. In this way, the lattice gas model is mapped to the Ising model exactly. In App. 5.1, we included detail identifications of the parameters in the notation consistent within this thesis.

Another encouraging example is the residual entropy of square ice discussed by Lieb [47]. Consider a Lieb lattice, i.e., a square lattice with additional sites at the middle points of the edges of the square lattice. (These additional sites will be referred to as Lieb sites in this thesis.) Put oxygen atoms on the square lattice sites and put hydrogen atoms on the Lieb sites. If one assigns two neighbouring hydrogen atoms to each oxygen atom, then it forms a 2D square ice. There are various ways to assign the hydrogen atoms to the oxygen atoms, which leads to the residual entropy of square ice. Let us focus on one oxygen atom. If a hydrogen atom covalently bond with this oxygen atom, we put an arrow on the edge of the hydrogen atom pointing towards this oxygen atom; otherwise we put an arrow pointing in the opposite direction. If one neglects the ionisation effect, then each oxygen atom should have two arrows in and two arrows out, which is often referred to as ice rule in the literature. So, there are, in total, six allowed configurations for each oxygen site (see Fig. 2.1). Therefore, this model is also known as six-vertex model. For a given square ice, the

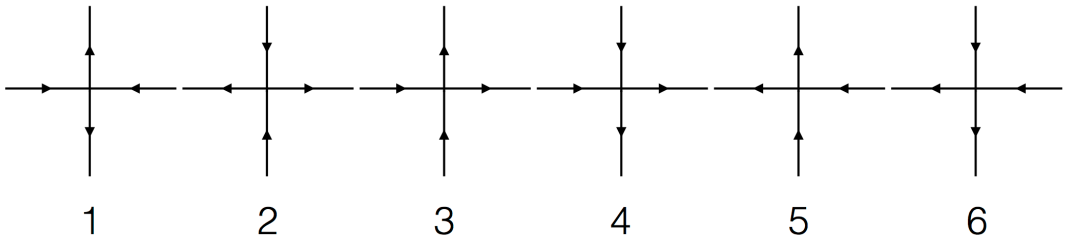

Figure 2.1: Square ice model: six allowed configurations of a vertex.

number of all possible configurations are computed exactly with the transfer matrix [47]. Lieb's 2D square ice model remained on the paper until it is realised in experiment recently by sandwiching water molecules betrween two sheets of graphene [5].

In Lieb's square ice model, the oxygen atoms are fixed on the square lattice sites, and the molecules cannot move. In order to study the hydrogen-bond interaction in water, we would like to define a model similar to Lee and Yang's lattice gas model where molecules are free to move, whereas the molecules retain degrees of freedom such that some version of the hydrogen-bond interaction may be defined.

Since the water molecule has a permanent dipole moment and the inter-molecule distance is comparable to the molecule size, one of the simplest choices for the molecule will be a physical dipole that consists of two equally charged monomers bonded together. We called it a dipolar dimer. There are various ways to arrange the dipoles. For example, one may put the dipoles on the lattice points and allow the dipoles to rotate. This model has been recently reported in experiment with organic molecules [24]. With frustrations, the dipoles are not oriented at low temperature, and form a quantum dipole liquid state according to Ref. [24]. However, this is not the model which we are looking for, because the dimers are not free to move spatially, which is more similar to Lieb's ice model.

To fix the dipole p_D of a dipolar dimer, we fix the length l_D of the dimer. Denote the polar charges $\pm q_D$, so we have

$$p_D = q_D l_D. \tag{2.6}$$

Instead of fixing the dimers on the lattice sites, we will put our dipolar dimers on the edges. To keep our model general, we shall consider a lattice L defined by its lattice sites (vertex set, V) and edges linking the lattice sites (edge set, E). More precisely, "lattice" as such is rather called a graph

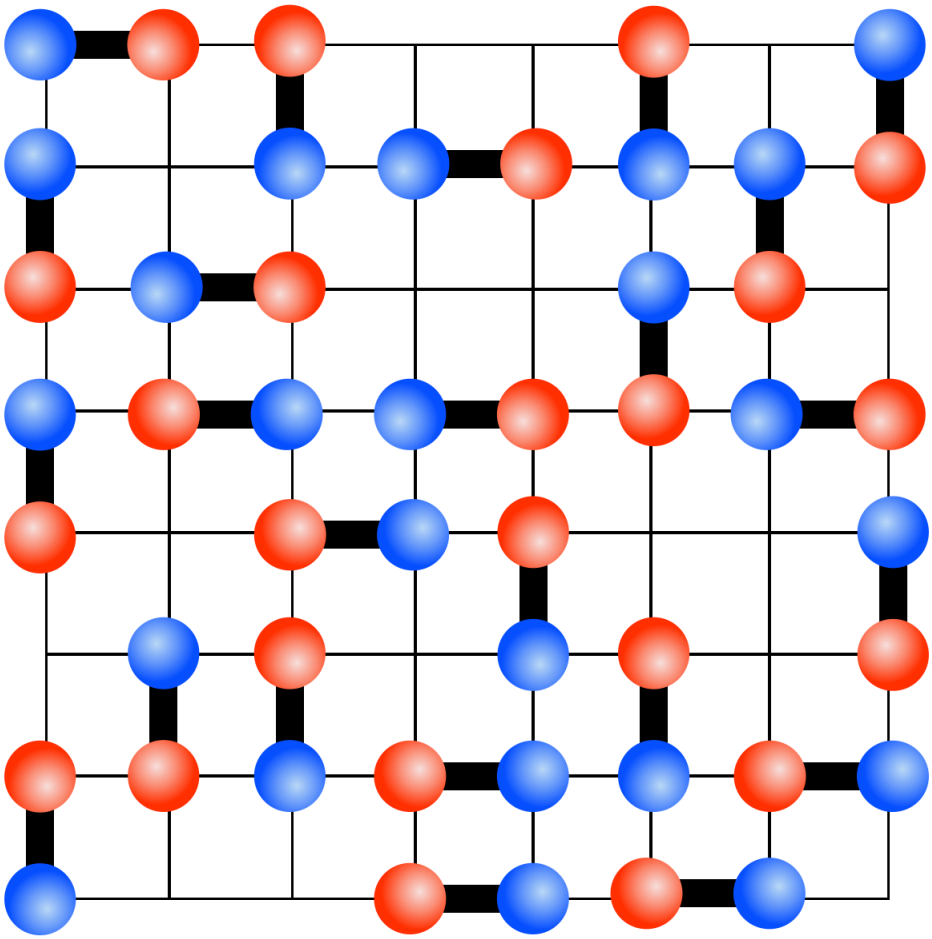

Figure 2.2: Dipolar dimer liquid on 2D square lattice.

in mathematics. In most physics context, we will consider $L = (V = \{v\}, E = \{e\})$ with the vertices being lattice points (in the mathematical sense) and the edges linking the neighbouring vertices. To avoid possible confusions with the random graphs that we will construct in Sec. 2.2, by abuse of language, we call $L = (V, E)$ a lattice.

Let the dimers cover the edges, i.e., two ending points of a dimer sit on the vertices of the lattice. Since all the dimers have the fixed length, dimers can only cover the edges with length matching the dimer length. This might not be the case, e.g., in the long range RVB model where two spins spatially far apart can still pair into a dimer. However, this is not a very restrictive condition. Many 2D and 3D lattices satisfy this condition, e.g., triangular lattice, square lattice, and honeycomb lattice in 2D as well as regular cubic lattice and rhombohedral lattice 3D, etc. Fig. 2.2 shows an example of the dipolar dimers on the 2D square lattice. To model the water in liquid phase, we shall adopt some ideas from the lattice gas model. Every dipolar dimer is allowed to move freely on

the lattice, whereas there is a hard-core repulsion if two dimers encounter, i.e., the dimers are not allowed to overlap.

It is the interactions between the dipolar dimers that make the system more interesting. At the relevant energy scale of 10^2meV as estimated above, the most important interaction is the hydrogen-bond interaction. Unlike the long range Coulomb interaction, the hydrogen bond can only happen when a positively charged hydrogen atom becomes close to some lone pair of a strong electronegative atom (e.g., nitrogen, oxygen or fluorine). So, we shall assign an attractive interaction if two dimers have their ending points of opposite charge sitting on the nearest neighbouring sites; otherwise we shall assign a repulsive interaction. This interaction rule has the same sign convention as the Coulomb's law. We shall call it Coulombic interaction in this thesis. It should be emphasise that this Coulombic interaction arises due to the hydrogen bonds, and it has different physical nature from the Coulomb interaction of the charges.

Mathematically, we may summarise the Hamiltonian as follows.

$$\begin{aligned} H_{DDL} &= \sum_{(a,b)} U(a,b), \\ U(a,b) &= \begin{cases} \infty, & \text{dimer } a \text{ and dimer } b \text{ overlap,} \\ J[N_+(a,b) - N_-(a,b)], & \text{dimer } a \text{ and dimer } b \text{ do not overlap,} \end{cases} \end{aligned} \tag{2.7}$$

where the sum is taken over all pairs, and $N_\pm(a,b)$ is the number of edges connecting nearest neighbouring points of two dimers with charges of the same sign $(+)$ or of the opposite sign $(-)$.

This completes our definition of the (classical) dipolar dimer liquid. This definition is very general, and it is easy to extend this model to more complicated cases. For example, if electrolytes are added to the water, one may include charged monomers. If the ions are hydrated, one may further include trimer, tetramer or other more complicated complexes. However, we shall not be too ambitious to expect that such an ideal model is comparable directly to the complicated real systems. If new energy scales emerge, new model should be constructed. In pure water, the self-ionisation effect is very small, and there are no ions from electrolytes, so we may well content ourselves with the charge neutral dipolar dimers. (So is it in Lieb's ice model.)

There are other interesting terms that may be included. In quantum (neutral) dimer model [64, 54], there is a kinetic term and an interaction term. The kinetic term is a local term with off-diagonal transition elements in the configuration space of the dimers, which allows the dimer to hop around. The interaction term is a face-to-face interaction between two parallel dimers diagonal in

the configuration space. The quantum dimer model may be stabilised in the staggered phase or the columnar phase in the presence of the interactions [54]. When the kinetic is large, the quantum fluctuation may induce a quantum solid-liquid transition, and the quantum dimers form a quantum liquid [54]. At room temperature, the kinetic energy of the water molecules is smaller than the hydrogen-bond interaction by a factor of five. In Sec. 2.2 we shall drop out this quantum term nor neglect the face-to-face interaction. It should be emphasised that dropping out this kinetic term does not mean to freeze out the motion of the molecules. Instead, various configurations of the dimers are taken into account in terms of a combinatoric quantity, which contributes significantly to the entropy as in the classical dimer model and in the square ice model. The classical limit of dropping the kinetic energy is analogous to the Hubbard model in the limit of $t = 0$, i.e., the strong interaction limit with flat bands. Then, it will not be surprise that the staggered phase and the columnar phase will help to understand dipolar dimer liquid.

In Sec. 2.2 we will show that there is liquid-liquid phase transition in the classical DDL by mapping the dipolar dimer liquid to some Ising model. In order to do so, we need an additional mild condition that the lattice L is bipartite. Mathematically, it means there exist two sets of vertices $V_A, V_B \subset V$, such that i) $V_A \cap V_B = \emptyset$, ii) $V_A \cup V_B = V$, iii) $\forall e \in E$, $\partial e \cap V_A \neq \emptyset$ and $\partial e \cap V_B \neq \emptyset$, where $\partial e = \{v_1(e), v_2(e)\}$ is the set of the ending points of the edge e. This condition simplifies our problem by excluding the frustrations. It is known that frustrations in dimer liquid will lead to other interesting physics, like the fractional excitations and topological orders. I believe there are similar effects in the quantum dipolar dimer liquid on non-bipartite lattices, which will be left for future researches.

Although our definition of the model is not restricted to 2D, but the statistical physics in 2D are much better known compared to higher dimensions. We will resort to various exact results (of 2D Ising model) to get insights in to the DDL. For example, we are able to prove the existence of a liquid-liquid phase transition and to bound the critical temperature quite tightly with the exactly solved Ising models on square and triangular lattice.

The generalisation of the DDL by including the quantum fluctuations and the face-to-face interaction of the quantum dimer model will be discussed in Sec. 2.4. This extension might be beyond our original scope of modeling water, but it is quite interesting in physics by itself. Another interesting extension is to include the polymers motivated by the protein problems. In 2D, the configurational entropy of the dimer liquid can be evaluated exactly even in the presence of the polymers [89]. Comparison to MD simulations and recent progress in MD simulations will be commented in Sec. 2.5.

2.2 Glacia Phase and Annealed Ising Model on Random Graphs

In this section, we will discuss about classical DDL that contains only Coulombic interaction. Even though the model seems quite simple, there is some interesting physics. Particularly we will show that there exists a liquid-liquid phase transition. The low temperature phase is ordered but not solidified, which we named *glacia* phase. By constructing an exact mapping to Ising model, we are able to show that the order in glacia phase is equivalent to the magnetisation in Ising model, therefore the critical point is described by the same universality class of the *annealed Ising model on random graphs*. In 2D, the critical temperature can also be bounded quite tightly with the help of exactly solved Ising models.

Although the interaction in Eq. 2.7 appears innocent, it is not obvious how to handle it algebraically. It turns out to be helpful, instead of staring at the dimers, to look at the lattice $L = \{V, E\}$. Each vertex can only be in one of the three states, occupied by a positive charge, empty, or occupied by a negative charge. If two ending points of an edge $\partial e = \{v_1(e), v_2(e)\}$ are covered by two different dimers, then an interaction energy $\pm J$ is assign to that edge, where the sign depends on the charges on ∂e. It is a simple abstract of the hydrogen-bond interaction.

The infinite hard-core repulsion may be taken as a geometric constraint. Define the configuration space of the dipolar dimers $\mathcal{C}$ to be the set of configurations without any pair of dimers overlapping. Then, for a given allowed configuration $C \in \mathcal{C}$, we define the charge function on the lattice

$$Q(v|C) = \begin{cases} +1, & \text{if it is occupied by a positively charged atom,} \\ 0, & \text{if it is not occupied by any atom,} \\ -1, & \text{if it is occupied by a negatively charged atom.} \end{cases} \tag{2.8}$$

With the help of this charge function, we are able to rewrite the Hamiltonian of the DDL in Eq. 2.7 in a form more similar to that of an Ising model

$$H_Q(C) = \sum_{e \in E_{nn}} JQ(v_1(e|C))Q(v_2(e|C)), \tag{2.9}$$

where E_{nn} is a subset of E consisting of the edges linking the nearest neighbours. If L is bipartite lattice, $E_{nn} = E$. This Hamiltonian is diagonal in the configuration space of the dipolar dimers $\mathcal{C} = \{C\}$.

Although we are at the strong interaction limit compared to the quantum dimer model [64,

54], it is not obvious there exists a phase transition in the DDL. In quantum dimer model, the solid phase are stabilised by the face-to-face interaction. The columnar phase is preferred by the attractive dimers, and the staggered phase is preferred by the repulsive dimers [64, 54]. In DDL, the interaction depends on the orientations of the dimers. It has been proved by Heilmann and Lieb [25] that there is *NO* phase transition in the monomer-dimer system with only hard-core interaction. In Ref. [26], Heilmann and Lieb considered hard-core dimers with orientation preferred interaction, and they proved that there exists a phase transition where local rotational symmetry can be spontaneously broken. Heilmann and Lieb's model was proposed for the liquid crystals. Since the nearest neighbour Coulombic interaction in DDL as described by the Hamiltonian in Eq. 2.7 or Eq. 2.9 has no orientation preference, no nematic order would be expected. However, it is not impossible to have a liquid-liquid phase transition in DDL.

In reverse, if one *a priori* assumes that there exists an ordered phase, it is heuristic to speculate what is the order according to the Ising-like Hamiltonian in Eq. 2.9. More precisely, if one regards Q as spin variable, then $J > 0$ will support an antiferromagnetic order, i.e., the charge distributes alternatingly on the lattice .

It was Lieb who first pointed to the author in a private communication [51] that the existence of such an order in DDL may be proved by the Peierls contour argument in analogy to the Widom-Rowlinson model. The argument is summarised as follows. On a bipartite lattice, every dimer occupies an A site and a B site. Color the dimer [3] according to the color of its constituent monomer on A site. Then, the colored dimers do not interact with each other according to their charges, but interact according to their colors. The rule of the color interaction is simple: dimers of the same color attracts each other and dimers of different colors repels each other. After recoloring the dimers, the model looks similar to a lattice Widom-Rowlinson model, which is known to have a phase transition in dimension $d \geq 2$.

The remarkable ingredient in Lieb's proof is that the dipolar dimers can be categorised into two kinds, the "red ones" and the "blue ones". The dipolar dimers with the same "color" attract each other and the ones with different "colors" repel each other. This leads to the Widom-Rowlinson picture. The original model of Widom and Rowlinson's was proposed to understand the liquid-vapour transition [83]. For molecules with hard-core repulsion in the continuum, the existence of the phase transition in Widom-Rowlinson model was proved by Ruelle [65] (as pointed out in Ref. [51]); and on the lattice by Lebowitz ad Gallavotti [45].

[3] We follows the convention as illustrated in Fig. 2.2 that a positive charged atom is in red and a negatively charged atom is in blue.

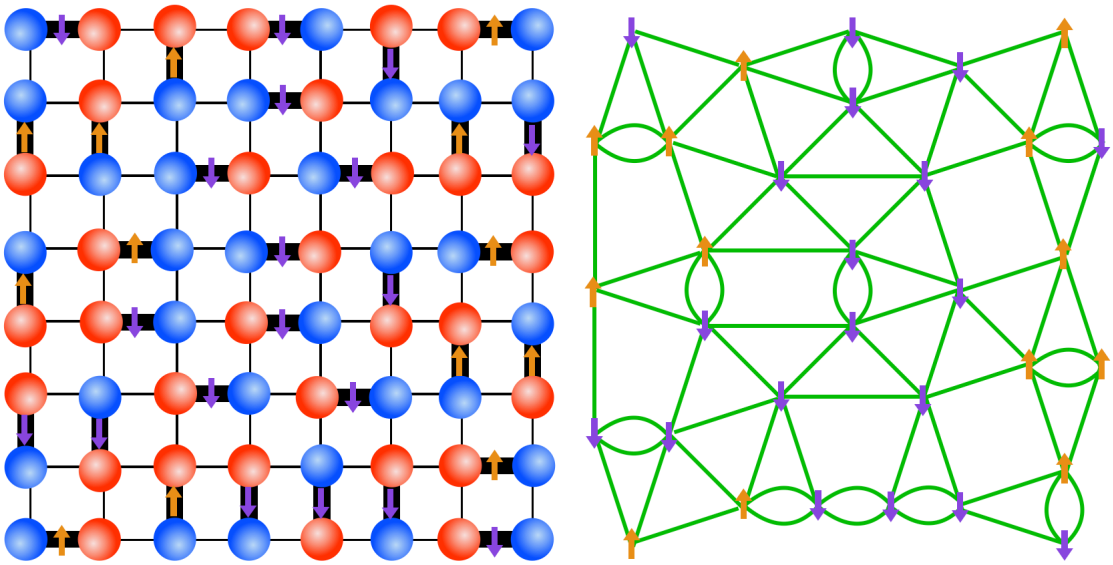

Figure 2.3: Dipolar dimer liquid on 2D square lattice and the Ising model on random graph constructed according to the dipolar dimer configuration.

Following this idea, I constructed an exact mapping from the DDL on bipartite lattice to the Ising model. It turns out that the Ising model so obtained is an annealed Ising model on random graphs. With this mapping, we are not only able to prove the existence of a phase transition, but also i) to identify the order parameter with the magnetisation of the Ising model, and ii) to bound the critical temperature with exactly solved Ising models. This exact mapping and the identification of the order parameter is valid in all dimensions provided the lattice is bipartite. Since the known exactly solved Ising models are mostly in 2D, so we will mainly focused on the 2D cases, particularly on the 2D square lattice as an example. In 3D, the critical behaviour should also be in some universality class of the Ising model according to our exact mapping. However, the 3D cases are less known. The method of the conformal bootstrap for the critical properties in 3D is also open by itself.

The detail construction is as follows. Consider a dipolar dimer on a bipartite lattice $L = \{V, E\}$, where the vertex set V has a natural partition $V = V_A \cup V_B$. If the dimer has its positively charged atom lying on a vertex of A type, one labels the dimer with a positive sign, otherwise one labels the dimer with a negative sign. [4] Each dimer must be either positive or negative. We augmented the lattice by adding the middle point of the edges $V_m(E)$. For example, in 2D, the square lattice is augmented to be the Lieb lattice. For a given dipolar dimer configuration C, we

[4] To avoid the confusion of the color and charge, here I used $\pm$ signs, which is equivalent to Lieb's color. These signs will become the spins up and down in the Ising model that we will construct.

take the middle points associated to the edges which are occupied by the dipolar dimers, and they form a subset $V_m(E|C)$ of the augmented vertex set $V_m(E)$. Then we put a spin on each vertex $v_m(e|C) \in V_m(E|C)$. If the dimer is labelled positive in the previous step, set the spin up; otherwise, set the spin down. For two given vertices $v_m(e_1|C)$ and $v_m(e_2|C)$, count the number edges spanning from ∂e_1 to ∂e_2 and draw the same amount of bonds $b_\alpha(C)$ spanning from $v_m(e_1|C)$ to $v_m(e_2|C)$. Therefore, we obtain a new diagram $\Gamma(C) = \{V_m(E|C), B(C)\}$, which depends on the dipolar dimer configuration C. With this construction, we map each dipolar dimer configuration to a random graph with specified spin orientations.

Fig. 2.3 shows an example of a given DDL configuration on the 2D square lattice mapped to Ising spins on a random graph generated according to the rules stated above. On 2D square lattice, the vertices can be classified by a sign $\sigma(v) = (-1)^{r(v)+c(v)}$ where $r(v)$ and $c(v)$ are the row number and column number of the vertex v respectively. For any dipolar dimer on edge e, the spin on $v_m(e|C)$ can be calculated $S(e) = \frac{1}{2}\sigma Q(\partial e)$. One notice that on the right hand side, it is independent of which ending point is used for calculating the spin orientation, therefore it is well-defined on the edge e.

Another consequence of this mapping worthy to be emphasised is that the random graph $\Gamma(C)$ generated by a dipolar dimer configuration C is in dependent of the orientation of the dimers, i.e., flipping a dipolar dimer on an edge does not change the topology of the graph generated. In terms of the Ising model, it is nothing but the fact that the spins are free to flip. Therefore the orientation degrees of freedom and the translational degrees of freedom are decoupled. The former is associated to the spin orientations while the later is associated to the connectivity of the random graphs. More precisely, we transcribe the DDL Hamiltonian in terms of the Ising model for a given dipolar dimer configuration C as

$$H_S(C) = -4 \sum_{b \in B(C)} JS(v_m^{(1)}(b))S(v_m^{(2)}(b)), \tag{2.10}$$

where $v_m^{(i)}(b)$ are the ending points of the bond b.

Define $D = [C]$ to be the dimer configuration obtained by neglecting the charges of the dimers in the configuration C. This identification is an equivalence relation π on $\mathcal{C}$, and dipolar dimer configuration splits $\mathcal{C} = \mathcal{D} \times \Sigma$, where Σ is the space of the orientations of the dimers provided an underlying dimer configuration D is given. The random graph $\Gamma(C)$ depends only on the equivalence

class $D = [C]$. With this notation, the partition function of the DDL becomes

$$Z = \sum_{C \in \mathcal{C}} \exp[-\beta H_S(C)] = \sum_{D \in \mathcal{D}} \left\{ \sum_{\{S(D)\} \in \Sigma} \exp[-\beta H_S] \right\}. \tag{2.11}$$

It is not difficult to recognise the term in the curly bracket in Eq. 2.11 is the partition of the Ising model on the random graph associated to the dimer configuration D. A more generic form of the partition function of the DDL is

$$Z = \sum_{D \in \mathcal{D}} W(D) Z_{\text{Ising}}(D), \tag{2.12}$$

where $W(D)$ is a weight factor proportional to the probability of the underlying dimer configuration D. If one assumes that all the dimer configurations are equally probable, it simply reduces to Eq. 2.11. If one includes the face-to-face interaction as in the quantum dimer model [64, 54], the stagger configuration swill be preferred for repulsive v and columnar configuration will be preferred in attractive v, and different configurations will have different weights.

The partition function of the form in Eq. 2.12 has a physical interpretation. If one regards the random graphs associated to the dimer configurations as disorder of the Ising coupling, then the partition function of the DDL Z is an average of the partition functions of the Ising models over various disorder configurations. This kind of disordered Ising model is often referred to as annealed Ising glass. [5] Nevertheless, it is much simpler in our case, because the random graphs do not really introduce frustrations by construction. So the couplings in our Ising models are always ferromagnetic. The randomness of the couplings is only due to the connectivity of the graphs, which is combinatoric. In 2D or higher dimensions, if the Ising models associated to the random graphs all have a phase transition, it is not surprising that the averaged model has a phase transition as well. In fact, one may further assert that the critical temperature of the averaged model should be bounded by the Ising models on random graphs with the maximal critical temperature and the minimal critical temperature.

This mapping also allows one to identify the order parameter. According to Eq. 2.9, it is intuitive to speculate that the configurations of low energy should have the charges of different signs close to each other. On a bipartite lattice, it is always possible to arrange the dipolar dimers in such

[5] The word *annealed* is used in contrast to another kind of disordered Ising model, *quenched* Ising glass, where the word quenched refers to averaging the free energy over various disorder configurations.

configurations by flipping each dimer locally. In this regard, one may define the order parameter as

$$\Phi = \frac{1}{2|V|} \sum_{v \in V} \sigma(v) Q(v), \tag{2.13}$$

However, it is not obvious that this kind of pattern may persist at finite temperature when the dimers are free to move, . The problem becomes simpler from the perspective of Ising model. By construction, this is exactly the magnetisation in the Ising model,

$$M = \frac{1}{|V|} \sum_{v_m \in V_m(E|C)} S(v_m). \tag{2.14}$$

It is not surprising to have a phase transition at finite temperature when the space dimension is no smaller than 2. In fact, the proof of the existence of the phase transition for the Widom-Rowlinson model by using the Peierls contour argument as pointed out by Lieb rings the bell of the homological proof for the Ising model.

In the low temperature phase, the dimers are arranged in a way such that the charges distribute on the lattice alternatingly. For example, on a 3D cubic lattice completely covered by the dipolar dimers, this charge order is similar to the ionic crystal of the salt NaCl. It looks like the hydrogen bond network in ice. But this phase is NOT ice as it has essential differences compared to the ice. In the 2D square ice model, the water molecules have only degrees of freedom of the resonant bonds but with the oxygen atoms pinned to the lattice. Therefore, the square ice model describes a solid with massive entropy. In DDL, the charge order forms mean while the dipolar dimers are still free to move. No translational or rotational symmetries are spontaneously broken. Therefore, the low temperature phase is also a liquid phase and this phase transition is a liquid-liquid phase transition. In this respect, we call this ice-like low temperature phase *glacia phase*, and this phase transition *glaica phase transition*.

Inspecting more details of this mapping, it turns out that more precise conclusions than the existence of the phase transition may be reached based on the knowledge about the Ising model. Particularly, Ising models on some 2D lattices are exactly solved, which may be used reversely to bound the critical temperature of the glacia phase transition.

First, it is heuristic to consider the mean field approximation. In the mean field approximation, the correlations of the fluctuation of the spins are neglected, and the problem reduces to a local problem of a single spin in an environment with its neighbours approximated by the average

alignment. The self-consistent equation reads

$$M = \frac{1}{2}\tanh(2\beta J z M), \tag{2.15}$$

where z is the coordination number, i.e., the number of neighbours that one spin has. It is well-known that the critical temperature is determined by the condition

$$\beta_c J z = 1. \tag{2.16}$$

The mean field approximation is only precise in the infinite-dimension limit, i.e., $z \to \infty$. When z is small, it tends to over estimate the order parameter. For example, in the case of 1D Ising model, $z = 2$ and the mean field approximation predicts a finite critical temperature, while the exact solution shows $T_c^G = 0$. In the DDL, although z fluctuates, it is natural to expect that when $\langle z \rangle$ is small, T_c drops to zero. So, the glacia phase only exists when the density of the DDL is not too small.

We shall now estimate the critical temperature of the DDL in the high density limit. A typical realisation of the configuration of the DDL completely covering the 2D square lattice is shown in Fig. 2.3. If one counts the number of neighbours surrounding a spin, it may various from four to six. These coordination number recalls the well-known results of the Ising model on square lattice ($z = 4$) and that on triangular lattice ($z = 6$). The former has a critical temperature $k_B T_c^{\square} = \frac{2J}{\ln(1+\sqrt{2})} \approx 2.2692J$ and the latter $k_B T_c^{\Delta} = \frac{4J}{\ln 3} \approx 3.6410J$. According to the mean field result Eq. 2.16, one expects that the former gives a lower bound and the latter gives a upper bound for the critical temperature of the DDL, i.e.,

$$2.2692J < k_B T_c^G < 3.6410J. \tag{2.17}$$

Notice that when two parallel dipolar dimers on the same plaquette, their interaction is $2J$ instead of J. In our construction, it is represented by the double bonds connecting two Ising spins on the random graphs. Rather counting the number of bounds for each vertex in the random graphs, one always finds six, i.e., the random graphs have all the vertices of degree 6. It implies that the critical temperature of the Ising model on triangular lattice $k_B T_c^G \lesssim 3.6410J$ may give a more precise bound. This estimation is confirmed with the numerical simulation. (See Sec. 2.3.)

In fact, the lower bound can be further improved by inspecting the low temperature excitations.

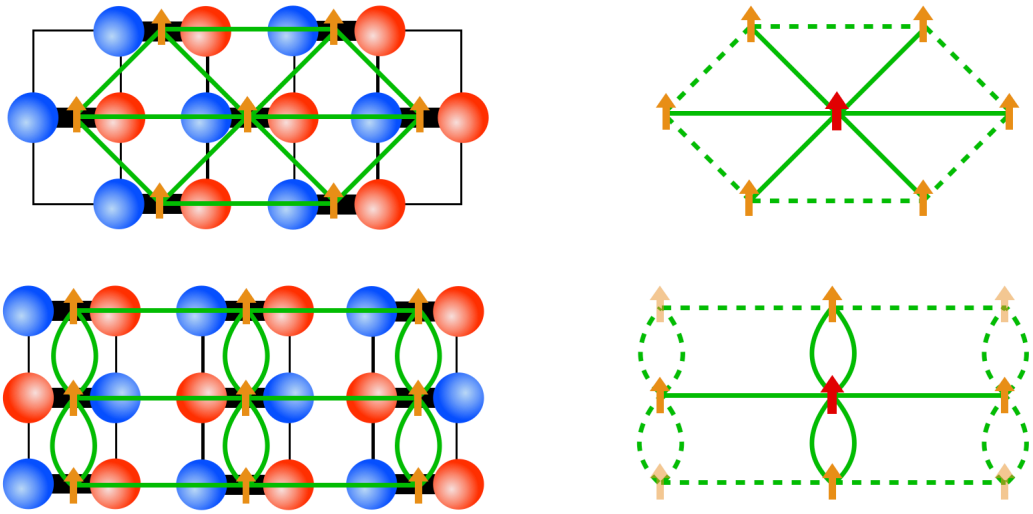

Figure 2.4: Staggered configuration and columnar configuration of the dipolar dimers.

The energy cost for flipping a spin is proportional to the number of bonds linked to a vertex Since all the vertices have degree 6, each single spin excitation then costs $6J$. If there are multiple spins flipped, the energy costs is proportional to the number of bounds crossing the domain wall. It two spins are linked by a double bond and are flipped together, it costs less energy for such kind of excitations than two separated spins flipped. Therefore, the more double bonds in a random graph the lower critical temperature the associated Ising model will have.

Two realisations of the dipolar dimers achieving the limit of no double bonds and the limit of maximal number of double bonds are shown in Fig. 2.4. Following the convention of quantum dimer model (neglecting the charge degrees of freedom of the dipolar dimers), I referred to the dimer configuration in the top panel as staggered configuration and to the one in the bottom panel as columnar configuration. In the staggered configuration, one finds that the associated random graph is exactly the triangular lattice and naturally there are no double bonds. It reconfirms our previous estimation from the mean field approximation, i.e., $k_B T_c^{\Delta}$ sets the upper bound. In the columnar configuration, each spin has four neighbours and two double bonds. Since each vertex is of degree 6 and each spin has to have at least four neighbours, it achieves the maximal possible number of double bonds. Therefore, it will sets the lower bound of the critical temperature. It is not difficult to observe that the associated Ising model is on a deformed square lattice, and the couplings in horizontal direction and in vertical direction are J and $2J$ respectively. Luckily, this Ising model is also exactly solved and its critical temperature is $k_B T_c^{\square hv} \approx 3.2820J$. (See Sec. 5.2, Eq. 5.11 in

Appendix.)

For a generic random graph constructed according to the dipolar dimer configuration, any vertex can have zero, one or two double bonds. If a vertex has one double bond, it can be regarded as a mixture of the staggered and the columnar configurations. Since the total partiition function of the dipolar dimer liquid is the average of the partition functions of the Ising model over various random graphs, the critical temperature of the glacia phase cannot exceed the range of the highest and the lowest critical temperature of the Ising models on two particular graphs we identified above. Therefore, we tighten the bound of the critical temperature to a quite small range

$$3.2820J < k_B T_c^G \lesssim 3.6410J. \tag{2.18}$$

It is known that there is a version of the Ising model on random graphs being solved exactly by Kazakov [34]. Kazakov's model has a critical temperature $k_B T_c^K = \frac{1}{\ln 2} J \approx 1.4427J$, which is far more loose than the bound we have in Eq. 2.18. The random graphs in Kazakov's model come from the planar Feynman diagrammes of some matrix model. However, at the dense limit of the DDL, it is not as useful as the estimation we have above, because the random graphs in Kazakov's model are somehow different from the random graphs we constructed. Particularly, in Kazakov's model, there are essential contributions from the random graphs whose plaquettes can be polygons of large number of edges. These graphs can only appear when the density of the DDL becomes lower according to our construction. Hence, it is not surprising that the critical temperature also becomes lower if the density is lower. Therefore, we expect that the glacia phase persists at finite temperature even at a lower density. Another interesting feature of the Kazakov's model is that the phase transition is a third order transition. We speculate that glacia transition of the DDL may soften at a lower density. Perhaps, there are other possible instabilities setting in (e.g., phase separation) before the glacia transition softens.

Another remark I would add here is that, at the time this thesis is written, it is reported that an evidence of second critical point of water is evidenced in MD simulations by Debenedetti *et al.* [14]. A liquid-liquid critical point was found in deeply supercooled water and this critical point seems consistent with the Ising universality class. At their condition, kinetic energy is small which matches our strong interaction approximation in our model of DDL. The low temperature phase is reported to be an ice-like phase, which also matches the glacia phase in the DDL. However, it is hard to compare two models directly. In the MD simulations, density was used as an order parameter. In our model, we have close packed DDL on a lattice, and the density is a constant. I believe that the

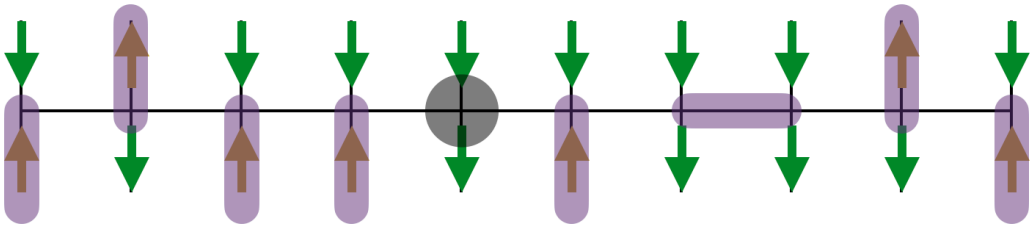

Figure 2.5: Lieb's representation of the dimer covering.

DDL does describe some important features of the liquid-liquid phase transition observed in the MD simulation. More detail comparison will be left for future researches.

2.3 Numerical Method of Simulations

The reasoning of the glacia phase transition in Sec. 2.2 has been confirmed numerically with Monte Carlo (MC) simulations. When the dimers completely covers the 2D square lattice the simplest non-trivial dimer move is the two-dimer reorientation (as the T_2 term in Eq. 2.20 in Sec. 2.4 for the quantum dimer model). However, it is known that the configuration space of the dimers on 2D square lattice splits into various topological sectors [64]. Even though T_2 is believed to be ergodic within each topological sector, one cannot reach a state in a different topological sector by applying T_2 once the initial state is given. Therefore, this intuitive choice of T_2 is not eligible for generating the Markov chain of the states for the MC simulation. In other words, it implies a dynamical jamming transition, where the ergodicity of the system evolving under the Hamiltonian is broken, in the classical dimer model. It is direct to observe the fact that, with only T_2, the dimers are completely stuck in the staggered configuration .

To circumvent this difficulty, we may go back to Eq. 2.12, where the degrees of freedom of the random graphs and the spin configurations are decoupled. The former depends only on the underlying dimer configuration, while the latter is the spin states of a standard Ising model. Then, the only task remains is to sample the dimer configurations properly.

Lieb's solution of the dimer model on square lattice turns out to be very helpful for sampling the random graphs [48]. Lieb constructed another representation of the dimer model on square lattice [48], where the dimer configurations are mapped to an Ising model on a shifted lattice illustrated in Fig. 2.5.

In Ref. [48], Lieb mapped the dimer configurations row-by-row into an associated Ising model. Then, the partition function of the dimer model can be calculated as the restricted transfer matrix of the Ising model. An example of a matrix element of the transfer matrix and the corresponding dimer configuration is shown in Fig. 2.5. In fact, Lieb considered a monomer-dimer covering, which is more general than we need here. Lieb's construction rule can be summarised as follows. Consider a monomer-dimer covering problem on a 2D square lattice. One associate an Ising spin to the middle point of each vertical bond. For the top row, an additional row of vertical bonds should be added. In the periodic condition, these extended vertical bonds are shared with the first row. Then we put the dimers according to the spin configurations row by row. If one has an up spin on a vertical bond, one puts a dimer on that vertical bond. Then, there are only three possible transitions from an in-state to an out-state: 1) an up spin propagates vertically upwards with a down spin, or a down spin propagates with an up spin; 2) a down spin propagates with a down spin; and 3) two down spins copropagate with two down spins. In the first case, one needs to do nothing. In the second case, one puts a monomer on the vertex between these two down spins. In the third case, one puts a horizontal dimer on the vertices in the row sandwiched by these four down spins.

Obviously, it is not allowed to have an up spin propagating with an up spin, otherwise two vertical dimers will overlap on a vertex. In our case, we do not need monomers. We will respect the constraint that it is not allowed to have a down spin propagating with a down spin either. Since the partition function of the dimer system is

$$Z_D = \sum_{a_0,\ldots,a_m} T_{a_0,a_1} T_{a_1,a_2} T_{a_2,a_3} \ldots T_{a_{m-1},a_m}, \tag{2.19}$$

where a_i run through all the spin configurations in i-th row. [6] If one samples in the space of $\{a_i\}$, it is guaranteed to be ergodic in the space of dimer configurations, while this sampling is nothing but sampling the Ising model associated to the dimer model according to Lieb's construction in Ref [48].

Now, the sampling of the DDL is equivalent to the sampling of two coupled Ising models. The result of the MC simulation is shown in Fig. 2.6. One may estimate the critical temperature to be $k_B T_c^{G,MC} = (3.5 \pm 0.1)J$, which comfirms theoretical prediction in Eq. 2.18 without surprise.

[6] The subscript $a_0 = |\downarrow\downarrow\ldots\rangle$ if one has open boundary condition, or $a_0 \equiv a_m$ if one has periodic boundary condition in the vertical direction.

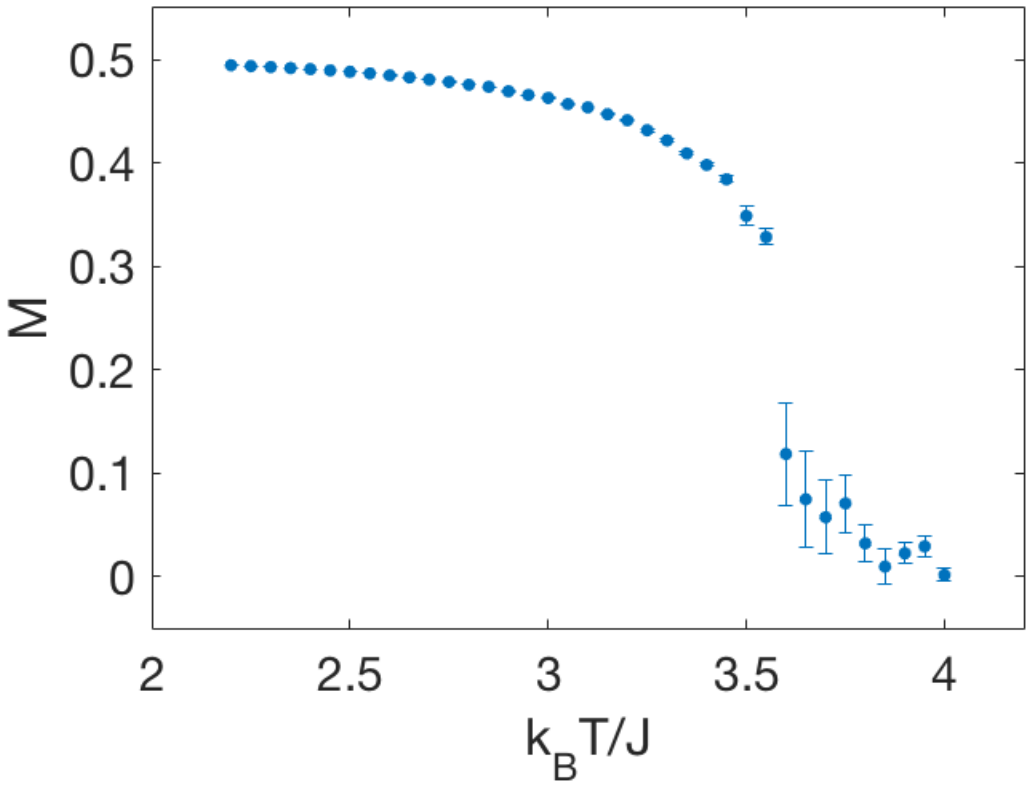

Figure 2.6: MC simulation of glacia phase transition.

2.4 Quantum Dipolar Dimer Liquid

In this section, we discuss about the generalisation of the classical DDL to a quantum DDL. The total Hamiltonian of the quantum DDL can be summarised pictorially as follows

$$
\begin{aligned}
H_{\mathrm{QDDL}} =& t_1 T_1 + t_2 T_2 + vV + JV_C, \\
T_1 =& |\ominus\!\!-\!\!\oplus\rangle\langle\oplus\!\!-\!\!\ominus|, \\
T_2 =& |\ \overline{\ }\ \rangle\langle|\ \ |\,| + |\,|\ \ |\rangle\langle\ \overline{\ }\ |, \\
V =& |\,|\ \ |\rangle\langle|\ \ |\,| + |\ \overline{\ }\ \rangle\langle\ \overline{\ }\ |, \\
V_C =& -|\ominus\cdots\oplus\rangle\langle\ominus\cdots\oplus| \\
&+|\oplus\cdots\oplus\rangle\langle\oplus\cdots\oplus| \\
&+|\ominus\cdots\ominus\rangle\langle\ominus\cdots\ominus|,
\end{aligned}
\tag{2.20}
$$

where t_1, t_2, v, J are the coupling constants. The last term JV_C is the DDL Hamiltonian defined in Eq. 2.7.

In the first term T_1, symbol $\oplus, \ominus$ represent the polar charges of a dipolar dimer and the short line stands for the dimer link. Therefore, T_1 flips the orientation of a dimer locally. It is trivial for neutral dimers but not for dipolar dimers. It can be considered as a single-dimer kinetic term for the dipolar dimers.

The second term and the third term are the same as the kinetic term and the face-to-face interaction term in quantum dimer model [53]. We adopt the same pictorial representation for the dipolar dimers with charges suppressed in this pictorial representation. Since V does not change dimer configurations, it has a natural extension from neutral dimers to dipolar dimers, i.e., it counts the interaction of two face-to-face dipolar dimers as if they are neutral dimer. This charge independent interaction can be consider as a short range extension of the (zero-range) hard core repulsion. It can be attractive $v < 0$ or repulsive $v > 0$. The extension of T_2 is a little more complicated. There can be two natural ways to extend this two-dimer reorientation term. 1) If one regards T_2 in the neutral dimer model as two-dimer reconnection, then the natural extension of T_2 will also reconnect ending points of the dipolar dimers and leave the charges of the dipolar dimers unmoved. However, this might not be always possible for any pair of dipolar dimers due to the charge neutral condition that requires each dimer to be neutral in total. In order that the reconnections respect the charge neutral

condition, one may further assume all those reconnections violating the charge neutral condition are of zero amplitude. This simple assumption introduces additional combinatoric restrictions for the transitions among the dipolar dimer configurations. 2) An alternative interpretation is to regard this term as two-dimer rotation. Then its has an extension to dipolar dimers without obstruction form charge neutral condition, whereas it inevitably changes the spatial charge distribution. To distinguish from the former case, we will denote this term as $\tilde{T}_2$ if we adopt this second way of extension.

The quantum DDL is also well defined on lattice at higher dimension or at other fillings. However, the associated Ising model are less known. Even though our construction of the exact mapping from the DDL to the Ising model on random graphs does not depend on details of the bipartite lattice L, and we can always apply the mapping, less quantitative information can be extracted from the Ising model side. Therefore, we will focus only on the close packed quantum DDL on 2D square lattice.

The term T_1 is a single-dimer flipping term. It turns out to have a simple interpretation in the picture of the Ising model described in Sec. 2.2. Since T_1 term is diagonal in $\mathcal{C}$, it only contribute to the $Z_{\text{Ising}}(C)$. With the notations we defined in Sec. 2.2, for a given C, T_1 may be transcribed as

$$t_1 T_1 \leftrightarrow t_1 H_{T_1}(C) = t_1 \sum_{v_m \in V_m(E|C)} |\bar{S}(v_m)\rangle\langle S(v_m)|, \tag{2.21}$$

where $\bar{S}(v_m)$ means flipping the spin $S(v_m)$ on vertex v_m. Therefore, combining Eq. 2.10 and Eq. 2.21, we have an Ising model on graph $\Gamma([C])$ with transverse field and t_1 is exactly the strength of the transverse field.

The second term T_2 in Eq. 2.20 is a two-dimer reorientation term. As described above, there are two ways to extend the two-dimer reorientation term from neutral dimer model to DDL. If one takes the reconnection T_2 that acts trivially on charge degrees of freedom, it does not allow the factorisation of the partition function as in Eq. 2.11 in general. But it does not introduce additional fluctuations for the spatial charge order either. In this sense, it is a weak coupling between the spatial charge order and the dimer motions. At low temperature $k_B T \ll J$, the spatial charge distribution is ordered. In this limit, the spatial charge order does not obstruct T_2, therefore T_2 becomes almost the same as it is for neutral dimer, and the partition function approximately factorises as in Eq. 2.11. At high temperature or large t_1 (in the spin disordered phase), the charge distribution does not have long range order, and there are strong local charge fluctuations. The combinatoric obstruction from the charge neutral condition can not completely suppress T_2. We expect when t_2 becomes much larger than $|v|$, the quantum DDL will still go through a quantum phase transition from solid to

liquid, though the critical value may be larger than that of the quantum dimer model.

If one takes the rotation $\tilde{T}_2$, then it disturbs both charge order and dimer configuration simultaneously. In quantum dimer model, RVB liquid phase is stabilised by this quantum fluctuation and a solid-liquid transition happens at Rokhsar-Kivelson point [64] $t_2 \sim v$. However, when J is much larger than v and t_2, the fluctuation of dimer configuration is suppressed by charge order. The gain of energy for the state of disordered dimer configuration by this fluctuation is about $\frac{t_2^2}{J}$ in stead of t_2. So a transition of ordered dimer configuration to disordered dimer configuration will happen around $\sqrt{vJ}$ in analogy to the Rokhsar-Kivelson point. It should be emphasised that the spatial charge order of the DDL persists over this phase transition. If t_1 is much larger than J, the spatial charge distribution is disordered according to the associated Ising model. In this case $\tilde{T}_2$ will be much less suppressed. Although t_1 is only a disorder field for the Ising model and not directly coupled to the dimer motions, it drives both quantum phase transitions of the spatial charge order and the dimer configuration order in the DDL.

2.5 Conclusion and Discussion

We proposed a new dimer model, DDL, which consists of dipolar dimers. It has Coulombic interaction between the dipolar dimers, which is an idealised model motivated by the hydrogen-bond interaction. Independent of the dimer configuration order, the DDL may exhibit a spatial charge order. We called the charge ordered phase glacia phase. We constructed exact mapping of the DDL to the annealed Ising model on random graphs, which helps to understand various properties of the DDL and its quantum generalisation. Particularly, in 2D, we are able to bound the critical temperature of the spatial charge order quite precisely with the help of various exactly solvable Ising models.

We discussed the effects of quantum fluctuations. In our construction, the single-dimer flipping is exactly mapped to the transverse field in the Ising model on random graphs. Furthermore, the spatial charge order and dimer configuration order are coupled. We argued that in the regime of strong Coulombic interaction, the charge fluctuation due to the single-dimer flipping may induce quantum phase transitions for both orders.

Although the Coulombic interaction does not prefer particular dimer configuration, it can help stabilise the solid phase by suppressing the quantum fluctuations of the dimer configuration. In real systems, a manifestation of this effect is the well-known fact that water, hydrogen fluoride and ammonia have higher melting point compared to the other compounds in their respective families

due to the hydrogen bonds in spite of their relatively small molecular weights. At finite temperature, it has been recently reported that the solid columnar phase melts undergoing a KT transition for classical dimer model [4]. It is then intriguing to study how the Coulombic interaction in DDL will modify the critical exponents, which we leave for future researchers.

The hydrogen-bond interaction endows water some distinguishing features. The hydrophobic effect and anomalous thermal expansion are believed to be related to the "hydrogen bond network" formed by the water molecules in the liquid phase according to MD simulations. More recently, it has been reported that MD simulations indicate a two-critical-point scenario of water [14]. In Ref. [14], an unusual critical point for a liquid-liquid phase transition is evidenced to be in the Ising universality class. It seems that various features of this newly discovered liquid-liquid phase transition in the MD simulations match the spatial charge order phase transition of the DDL. Although we have constructed an exact mapping of the DDL to the annealed Ising model on random graphs, a direct comparison between the DDL and the more realistic models in MD simulations is hard. The critical exponents may be good indicators to test this speculation, which we will also leave for future researches.

Before closing this chapter, it deserves to mention some recent progresses in MD simulations [91] and in protein folding problem [70, 16]. In both cases, the method of *deep learning* has been implemented for bio-physico-chemical systems. It becomes possible to achieve high-enough precisions only recently due to the rapid development of the computation power. Nevertheless, these success of the numerical methods does not diminish the meaning of the model study. Even though the training data of the Deep Potential come from the ab initio calculations and density functional theory, the "force field" becomes a black box. From an alternative perspective, perhaps the conventional concept of the force field is no longer a good picture to understand the complicated systems. In the protein folding problem, from electronic structure of the amino acids to protein quaternary structure, multiple scales are involved. The machine trained by deep learning can well be taken as a good phenomenological theory. As Laudau's theory of phase transition, one may start from it and apply it to magnetism, superconductivity, turbulence, etc.; one may also connect it to some microscopic theory and achieve deeper understanding of the physics. Attempts to deconstruction the black box is underway, e.g., Ref. [28], which might help us to handle the complicated systems with multiple scales.

Chapter 3

Topological Metamaterials with Odd Elasticity

The Vicsek model described in Chap. 1 demonstrates that active system may behave in a quite different way compared to solid materials. Contre the dictation of the Mermin-Wagner-Hohenberg theorem, a long-range order may establish even in 2D. A continuum model describing the flocks merging the Ginsburg-Landau theory and the Navier-Stokes theory has been proposed by Toner and Tu [78]. It demonstrates that concepts developed in solid materials may help us to understand various complicated systems. In some cases, the concepts borrowed from solid materials may require proper extensions.

It is heuristic to observe some important features from the active fluid. The Toner-Tu system can be considered as a combination of the Ginsburg-Landau theory and the Navier-Stokes equation. In Sec. 3.1, we first briefly review several intriguing points of the Navier-Stokes equation. In the "dissipationless" limit, the Navier-Stokes equation may still dissipate energy, while in the "dissipation" limit, the Navier-Stokes equation restores the time-reversal symmetry. In order that the small active particles are able to swim in water, the way they swim has to break the time-reversal symmetry. More interestingly, in Toner-Tu system, the active fluid may form a spontaneous chiral current, and it has been shown that the chiral current may leads to some topological modes of sound waves in analogy to the quantum Hall effect [73].

On the other hand, in analogy to the Hall viscosity, it is natural to consider the odd elasticity [67] in some active material if the stress responses to the strain instead of the strain rate. Notice that the odd elasticity violates the energy conservation. In the presence of the odd elasticity, the dynamics

of the system becomes non-Hermitian,

In Sec. 3.3, a 1D rotor chain connected by metabeams with odd elasticity is discussed. This rotor chain may be considered as a generalisation of the Su-Schrieffer-Heeger (SSH) model [31] with non-Hermitian dynamics. The 1D rotor chain admits topological modes. In order to discuss the topological feature, the definition of the Brillouin zone should be generalised [87, 93], and the definition of the Zak-Berry phase needs to be clarified [71, 93]. Similar to the non-Hermitian electronic systems, the bulk modes are localised, which is referred to as non-Hermitian skin effect [41, 86, 93]. The generalisations in 2D are discussed in Sec. 3.4.

3.1 From Navier-Stokes Equation to Active Matter

Classical hydrodynamics is governed by the Navier-Stokes equation (Eq. 1.6). It is known that turbulence often occurs when the flow is fast. Mathematically this arises due to the non-linear convection term in the Navier-Stokes equation. On the contrary, if one neglects the convection term and the pressure term, the Navier-Stokes equation reduces to a simple linear equation same as the heat equation, i.e., the viscosity term describes the diffusion of the velocity. To quantify the strengths of the convection (inertial) term and dissipation, with simple dimensional analysis, one may introduce a dimensionless ratio

$$\mathrm{Re} = \frac{U/L}{\eta/L^2} = \frac{UL}{\eta}, \tag{3.1}$$

where U and L are typical scales of velocity and length in the system. The number Re is called Reynolds number.

Turbulence tends to occur at high Reynolds number. This can happen 1) when η is small, and 2) when UL is large. This categorisation is not mathematical, since with proper nondimensionalisation, both cases mean a large Reynolds number Re. It is somehow intuitive to guide the physical designs. Controlling U and L in an experiment setup is often achievable, for example, in the wind tunnel experiments, while varying η over orders of magnitude can be harder for a given fluid.

Physicists apply statistical methods for studying turbulence [52]. Mathematicians resort to some different ways. An interesting limit is to take $\eta \to 0$, which leads to large Reynolds number with finite U and L. If one naïvely sets the viscosity $\eta = 0$, the Navier-Stokes equation reduces to the

Euler equation

$$\partial_t(u^i) + u^j\partial_j(u^i) = -\delta^{ij}\partial_j\tilde{p}. \tag{3.2}$$

The Euler equation is much simpler than the Navier-Stokes equation. By taking the curl, one may get rid of the potential term. Instead, one obtains a set of equation for the velocity $\mathbf{u}$ and the vorticity $\boldsymbol{\omega}$. With the help of this transformation, it is possible to prove the long term existence of the solution for the $2D$ incompressible flow for the Euler equation [18].

Nevertheless, this is not the happy ending of the fairy tale. The limit of $\eta \to 0$ is singular for the Navier-Stokes equation, as the viscosity term contains the highest order derivative in the equation. Therefore, in the limit of $\eta \to 0$, a solution of Navier-Stokes equation may not converge to a solution of Euler's equation in a simple way. Onsager argued [56] that there exist weak solutions to the Euler equation violating the energy conservation with Hölder regularity C^α less than or equal to the threshold $\hat{\alpha} = \frac{1}{3}$, which is now often referred to as Onsager's conjecture. It is still an active research direction in mathematics. The positive part of the conjecture, i.e., weak solutions with Hölder regularity better than $\hat{\alpha} = \frac{1}{3}$ conserves the energy, was proved by Eyink [17] and Constantin, E, and Titi [13] in 1994; while the negative part was proved quite recently by Isett [29] based on the method of convex integration developed by De Lellis and Székelyhidi (see Ref. [12], Ref. [29], and references listed therein). This method has also been applied for proving non-uniqueness of weak solutions to the Navier-Stokes equation by Buckmaster and Vicol [11].

If one considers more regular flows without turbulence, some exact solutions are known. For example, consider a laminar flow along x-direction between two infinite parallel plates perpendicular to the y-axis with distance H apart. If we look for a solution in dependent of x and z, one can solve the velocity profile in y direction [44]

$$u_x(y) = -\frac{G}{2\eta}y(y-H), \tag{3.3}$$

where G is the negative pressure gradient along the x direction. This configuration is often referred to as plane Poiseuille flow. The velocity profile is a parabolic dome with maximal at $y = H/2$ and vanishing at $y = 0, H$. Recently, Ilani's group and collaborators reported that electrons in graphene can be controllably tuned from ballistic regime to the Poiseuille regime [76]. The spatial resolved voltage and current profile is mapped by a single electron transistor mounted on the tip of a scanning probe [15].

Electrons are charged particles. A more general theory of hydrodynamics for fluids consisting of charged particles is called magnetohydrodynamics, where the Maxwell equation and the Navier-Stokes equation should be considered simultaneously. The magnetohydrodynamics is crucial for understanding various phenomena, e.g. the corona of the Sun, stability of magnetically confined plasma, etc. I will not discuss about the magnetohydrodynamics in this thesis. Nevertheless, the charge degree of freedom does allow one to manipulate the electrons with electric and magnetic fields. In most cases for electrons in solids or ions in liquids, problems can be simplified.

A particular example is the Hall effect, where a background magnetic field is applied to the system. Since the magnetic field break the time-reversal symmetry, the Hall fluid has some distinguished properties. One may consider a more general response of the stress due to the viscosity.

$$T_{ab} = \eta_{abcd}\mathcal{S}[\delta^{ce}\partial_e u^d]. \tag{3.4}$$

where the stress tensor T_{ab} can always be chosen to be symmetric [43]. Therefore, the viscosity tensor η_{abcd} splits into symmetric and antisymmetric parts with respect to the pair of first two indices and the pair of last two indices. If we further assume the fluid is isotropic, the most general form of the viscosity tensor is

$$\begin{aligned} \eta_{abcd} =& \eta\left(\delta_{ac}\delta_{bd} + \delta_{ad}\delta_{bc} - \frac{2}{3}\delta_{ab}\delta_{cd}\right) + \zeta\delta_{ab}\delta_{cd} + \eta^A E_{abcd}, \\ E_{abcd} =& \frac{1}{2}(\epsilon_{ac}\delta_{bd} + \epsilon_{ad}\delta_{bc} + \epsilon_{bc}\delta_{ad} + \epsilon_{bd}\delta_{ac}). \end{aligned} \tag{3.5}$$

For an incompressible flow, ζ can be set to zero, and η is the shear viscosity same as the one we have in Eq. 1.8. In Ref. [7], it is pointed out that the antisymmetric component η^A can also be non-vanishing when the time-reversal symmetry is broken. As this term is considered for the Hall fluid Ref. [7], it is called Hall viscosity. In quantum Hall fluid, the Hall viscosity has a quantum origin, and it is proportional to the shift [62, 63, 60].

Back to the Navier-Stokes equation, let us consider a red blood cell in blood vessels. The typical size of a red blood cell is about 10^{-5}m. The kinematic viscosity of water is of the order $10^{-6}\mathrm{m}^2\cdot\mathrm{s}^{-1}$. The typical velocity of the blood flow in vein or artery is about $0.2\mathrm{m}\cdot\mathrm{s}^{-1}$, and that in capillaries can be three orders of magnitude smaller. The Re estimated for a blood cell in blood vessels ranges from 10^{-3} to 2. Flows in this regime are often referred to as flows with low Reynolds number. The Navier-Stokes equation simplifies significantly as the non-linear convection term may be dropped out. The resulting equation together with the incompressibility equation is also called Stokes equations,

and the flows are also called Stokes flows. The Stokes flow has time-reversal symmetry, but it is not dull. An impressive experiment has been demonstrated by Heller where a drop of dye in Couette viscometer mixed with the rest of the liquid can be unmixed if one reverses the rotation [27]. A non-trivial consequence of this nontrivial time reversibility is vividly summarised as Purcell's scallop theorem, i.e., a scallop cannot move forward if it swims with a periodic motion and the motion is reversible in time in each period. The approximation of the Stokes flow is often a good approximation for microbes in water or in many other biological context. According to Purcell's scallop theorem, if a bacteria or a sperm would like to swim actively, one has to whip tits flagella in a way not reversible in time or to spin the tail in a helical motion. The mechanical energy is not conserved in these motions. In fact, these motions are energised chemically by ATP (or in some systems by proton pump). So if one consider a fluid made of active particles, the active energy pumping also needs to be taken in to account.

On a quite different scale, similar physics may happens. The collection motions of the flocks can be abstracted as a fluid of self-propelling particles. More interestingly, the flocks described by Toner-Tu equation [78] may have a spontaneous flow (breaking the time-reversal symmetry) similar to the phase transition described by the Ginsburg-Landau theory. More precisely, in Ref. [73], it is shown that the Toner-Tu equation for self-propelled particles in the overdamped regime reduces to

$$\begin{aligned} &\partial_t(\rho) + v_0\partial_j(\rho p^j) = D_\rho \Delta\rho, \\ &\partial_t(p^i) + \lambda v_0 p^j \partial_j(\rho p^i) = (\alpha - \beta|\mathbf{p}|^2)p^i - \tilde{v}_1\nabla\rho + \eta\Delta p^i, \end{aligned} \tag{3.6}$$

where ρ is the density of active particles, $\mathbf{p}$ is the local velocity polarisation of the active fluid, and v_0 is the local mean speed. The details of the derivation may be found in Ref. [73] and the references therein. However, it is worthy to emphasise that the first term containing coefficient α and β on the right hand side of Eq. 3.6 in second the line is of the form of Ginsburg-Landau free energy. The order parameter is the local velocity polarisation. In the symmetry-broken phase, the active fluid form spontaneous flow. In Ref. [73] it has also been shown that the coupled channels can be designed in a way to guide a chiral spontaneous flow. In analogy to the quantum Hall effect, it leads to the topological sound waves.

Before closing this section, I will also discuss about elastic active metamaterials. In contrast to Eq. 3.4, in elastic material, the stress tensor response with respect to the strain instead of the strain

rate, and up to linear terms we have

$$T_{ab} = C_{abcd}\mathcal{S}[\delta^{ce}\partial_e q^d], \tag{3.7}$$

where (C_{abcd}) is the elastic modulus tensor [43]. If we assume that the metamaterial is isotropic, one has a decomposition of elastic modulus similar to that of the viscosity tensor (Eq. 3.5)

$$C_{abcd} = M\left(\delta_{ac}\delta_{bd} + \delta_{ad}\delta_{bc} - \frac{2}{3}\delta_{ab}\delta_{cd}\right) + K\delta_{ab}\delta_{cd} + K^o E_{abcd}, \tag{3.8}$$

where M is the shear modulus, K is the bulk modulus, and K^o is the odd elasticity [67]. The odd elasticity term does not appear in the expansion of the free energy in quadratics of the strains [43], because it does not conserve the energy. Therefore, this term is only possible when there is an energy pumping in the system or the system is driven by external force, which is not forbidden in principle in active metamaterials. In Sec. 3.2, we will describe a model of metabeams with odd elasticity [67]. Then, we substitute the metabeams for the springs in a mechanical SSH model. It turns out that the topologically protected modes can still appear. In order to describe the topological features, one has to generalise the usual notion of the topology for the systems described by some non-Hermitian dynamics.

3.2 Topological Modes: Beyond the Electrons in Solids

Topological phases of matter has been one of the main topics over the past three decades. Most discussions are based on electrons in solids with prototype that can be dated back to SSH model or quantum Hall effect.

Quantum simulator of cold atoms provides a non-electron platform with great tunability. Since the atoms are neutral, they do not couple to the magnetic field directly. In order to realise the topological phase as the quantum Hall state, one may synthesise an effective gauge field with the help of the Berry phase (cf. Ref. [88] and references listed there). Analogy of Haldane's model has been achieved experimentally with cold atoms [30]. In a similar spirit, artificial gauge fields can also be engineered for photons, which has been demonstrated experimentally in Ref. [68]. Protocols to realise the fractional quantum Hall states with high fidelity has also been proposed [90]. In Ref. [90], the effective magnetic field is achieved by making the atoms rotate. Instead of stirring the atoms, one injects the angular momentum by two-photon adiabatic Raman transition. The experimental

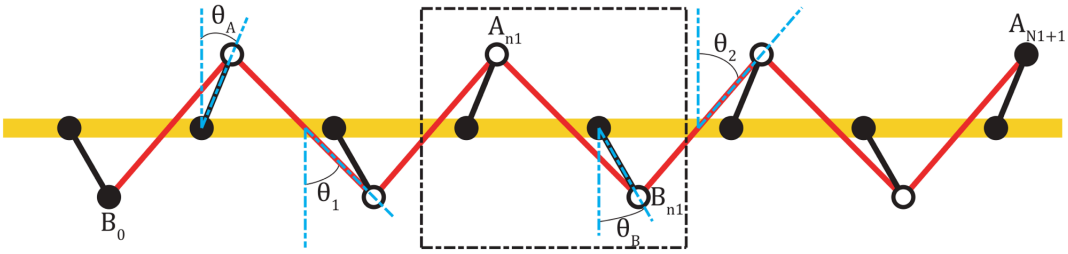

Figure 3.1: One dimensional rotor chain with metabeams.

realisation still remains for future researches.

Another analogy of Haldane's model was proposed in photonic crystals [61, 22]. The photon dispersion in a triangular lattice has a pair of Dirac points at the Brillouin zone corner. The Dirac points are well separated from other TE and TM modes. Raghu and Haldane proposed to open a topologically nontrivial gap with the Faraday-effect that breaks the time-reversal symmetry. Consequently, at the edges of the photonic crystal, there exist "chiral" photon edge modes similar to the edge states in the quantum Hall effect. An interesting application has been demonstrated in Ref. [15, 76], where lasing modes are protected topologically against the defect scattering.

Active fluid can also be made topological [73]. In Sec. 3.1, we see that the active fluid may form spontaneous flow. If one guides the flow with a superlattice of annuli, one obtains a vortex lattice [73]. The vortices plays a rôle of magnetic field. If there is a net flux, the collective modes of the fluid is then coupled to a background flow that breaks the time-reversal symmetry, Therefore, the topological sound modes emerges.

In spite of various interesting demonstration of realising quantum Hall analogues without electrons, in this thesis we will follow another track of topological model prototyped by SSH model. The 1D SSH model was originally proposed for understanding solitons in polyacetylene [75]. In SSH model, the topological modes are a half of the degrees of freedom of a unit cell localised at each ending of a chain. The Haldane chain [20]/AKLT model [2] and the Kitaev chain [36] also fall in this category. The edge modes consist of a half of a spin-1 (i.e., a spin-$\frac{1}{2}$) and a half of a charged fermion (i.e., a Majorana) respectively.

Recently, an intriguing analogy to the SSH model in the mechanical system was discussed by Kane and Lubensky [31]. Topological floppy modes in quasicrystals and disordered networks were discussed in Ref. [94] and Ref. [95]. Since our 1D rotor chain (Sec. 3.3) will be related to Kane and Lubensky's model, I will describe the latter in more details here. Let us consider a chain (along x-

axis) of evenly spaced rotors with their moving ends connected by a spring. Fig. 3.1 shows a typical configuration of the rotors. The angular position of the rotor on site n is measured from positive y-direction if n is odd, and from negative y-direction if n is even. If all the rotors are at the angular position $\theta_n = 0$ in the equilibrium state, it corresponds to the gapless point of this mechanical SSH model. If the rotors are tilted at an angular position $\theta_n = \langle\theta\rangle > 0$ in the equilibrium state, there exists another equilibrium state with $\theta_n = -\langle\theta\rangle < 0$. This is analogous to the two-fold degenerated gapped ground states for an infinite SSH chain.

The dynamics of the 1D rotor chain is described by Newton's law. Near the equilibrium configuration one has the linearised equation of motion

$$\ddot{\theta}_n = \sum_m D_{n,m}\theta_m, \tag{3.9}$$

where D is called dynamic matrix. The dynamic matrix D is semi-positive for a stable equilibrium configuration. A naïve counting degrees of freedom leads to $\nu = N_f - N_b$, where N_f is the number of rotors and N_b is the number of springs. A tentative physical interpretation of ν is the number of zeros modes N_0. This intuitive picture is not exact, but quite close. There can be states of self-stress which make the springs stretched or compressed without net force acting on the rotors. So, more precisely, $\nu = N_0 - N_{ss}$, where N_{ss} counts the number of states of self-stress.

The origin of these zero modes and the states of self-stress can be understood mathematically in a way similar to the flat band in an imbalanced bipartite lattice according to Lieb [49, 50]. Kane and Lubensky [31] factorised the dynamic matrix as $D = QQ^T$ and rewrote the equation of motion in a first order form with a Hamiltonian-like matrix

$$H = \begin{pmatrix} 0 & Q \\ Q^T & 0 \end{pmatrix}. \tag{3.10}$$

Then, ν can be related to the index of Q as

$$\nu = \operatorname{Ind} Q = \dim\ker Q^T - \dim\ker Q. \tag{3.11}$$

In Ref. [31], it has also been shown that the topologically protected zeros modes are related to the winding number

$$n = \frac{1}{2\pi\mathrm{i}} \int \mathrm{d}k \operatorname{Tr}\left[Q^{-1}(k)\nabla_k Q(k)\right]. \tag{3.12}$$

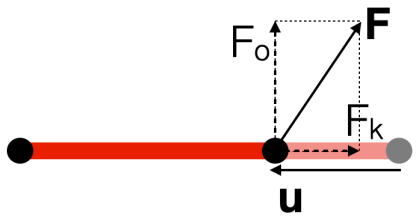

Figure 3.2: Metabeams with odd elasticity.

In Sec. 3.1, we have seen that the active matter may admit a term of odd elasticity (Eq. 3.8) that does not appear in the usual electronic systems. Since the odd elasticity violates the energy conservation, it is only possible in a system with active energy pumping, which is the case for many biological systems. In Sec. 3.3 we will define a generalised SSH model with odd elasticity arising from some metabeam as described in Ref. [67]. It is intriguing to study how the odd elasticity will modify the properties of a topological system. It turns out that such a system breaks the $\mathcal{PT}$ and has a complex spectrum in general. Therefore, a theory of non-Hermitian topological system is needed. The topological modes can still be well-defined, while the definitions of the Zak-Berry phase and winding number also need to be properly generalised. The bulk modes are modified by the non-Hermitian skin effect.

3.3 1D Rotor Chain with Odd Elasticity

In this section, a one-dimensional non-Hermitian generalisation of the SSH model is discussed. Same as in Ref. [31], we consider a 1D rotor chain, with massless rotors of radius r_0 attached to the equally spaced lattice points by ideal pivots, i.e. the rotors are free to rotate around the lattice points. Lattice points with rotors tilted upwards are called A sites, and those with rotors tilted downwards are called B sites. Connect the neighbouring tips of A and B rotors by the merabeams with odd elasticity.

The tilted angle with respect to the normal direction (upwards for A sites and downwards for B sites) are denoted as $\theta_{A,B}$ respectively as shown in Fig. 3.1. Denote $u_{A,B}$ the displacement of the rotors with respect to their equilibrium position respectively. We have

$$\begin{aligned} u_A =& |u_A|(\cos\theta_A, -\sin\theta_A)^T, \\ u_B =& |u_B|(\cos\theta_B, \sin\theta_B)^T. \end{aligned} \tag{3.13}$$

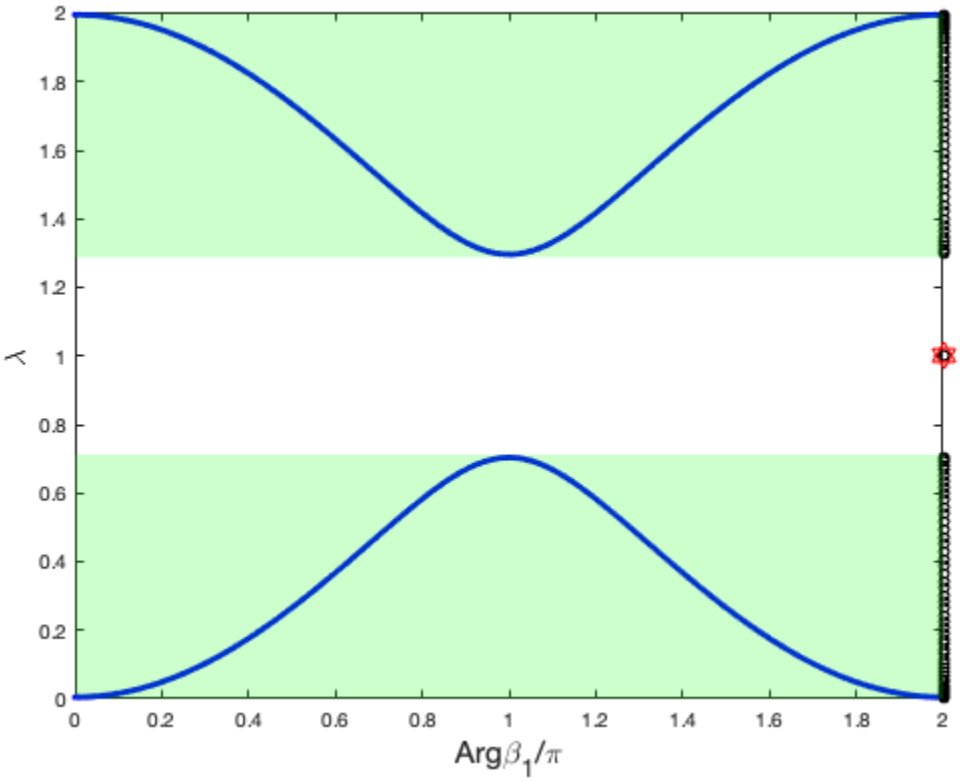

Figure 3.3: Spectrum of 1D rotor chain. The topological edge modes are indicated with red stars.

For small displacement, up to linear term the force of the metabeam can be written in the form of Hooke's law

$$F(u) = -(k\hat{n} + k^o\hat{\phi})(u \cdot \hat{n}), \tag{3.14}$$

where $\hat{n}$ is the unit vector along the metabeam and $\hat{\phi}$ is the unit vector of the transverse direction obtained by rotation $\hat{n}$ by 90 degrees counterclockwise. The first term containing k is evidently same as the usual spring constant, whereas the interesting new term containing k^o leads to the odd elasticity. For a metabeam connecting two neighbouring sites, we measure the angular position of $\hat{n}$ from the normal direction associated site on the right side and denote it by $\theta_{1,2}$. We shall emphasise here that the force of odd elasticity is not conservative. This is easy to be verified by considering the following cycle. First stretch the metabeam along radius direction, then rotation by a small angle while keep the length of the meta beam, after that squeeze the metabeam back to its original length, and finally rotate the metabeam back to its original position. In the first step and third step, as the

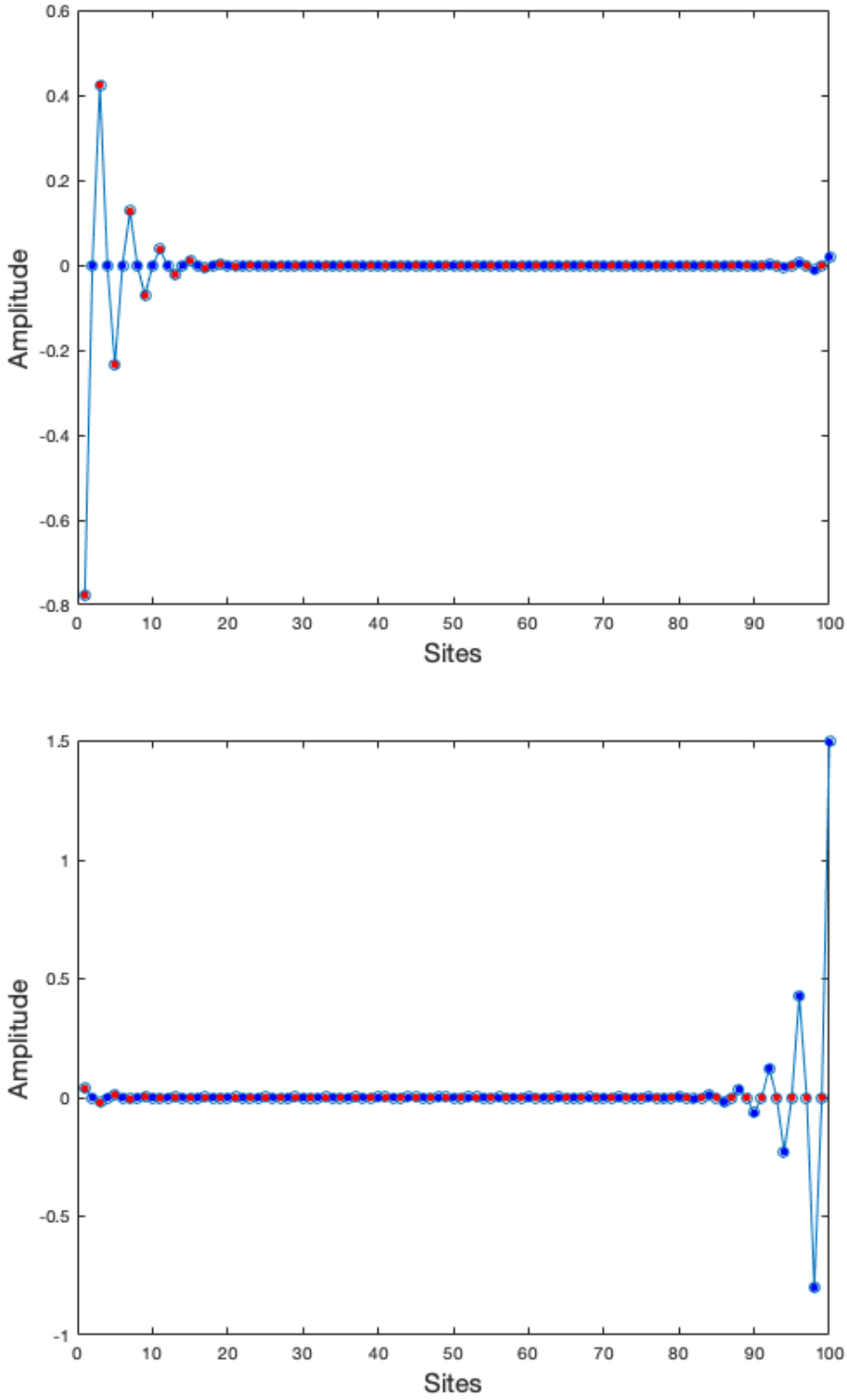

Figure 3.4: Two topological edge modes of 1D rotor chain.

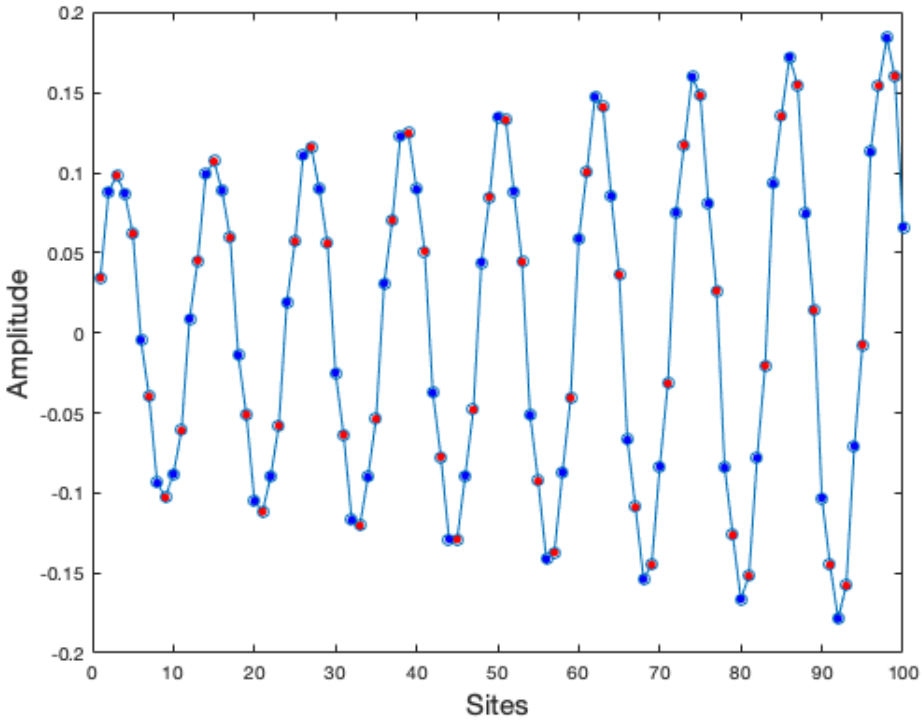

Figure 3.5: A typical bulk mode with non-Hermitian skin effect.

force of odd elasticity is perpendicular to the displacement, the energy change is due to the usual elastic force which is zero after the metabeam is squeezed back to its original length. However, in the second and fourth step, the work done by the odd elastic forces does not cancel. (Obviously, in step four, the meta beam resumes its original lenghth therefore no force on it at all.) As we discussed in Sec. 3.1, nonconservation of mechanical energy may naturally arise in biological systems as chemical energy may be used for driving rotational motions of flagella or molecular motors. The dynamics is then non-Hermitian.

Then the equation of motions for the system is given by Newton's law

$$\begin{aligned}
m\ddot{u}_{A,n} =& + c_1 u_{B,n-1} - a u_{A,n} + b u_{B,n},\\
m\ddot{u}_{B,n} =& + b' u_{A,n} - a' u_{B,n} + c_1' u_{A,n+1};\\
a =& (k + k^o \cot\Theta_A)\sin^2\Theta_A + (k - k^o\cot\Theta'_A)\sin^2\Theta'_A,\\
a' =& (k + k^o \cot\Theta_B)\sin^2\Theta_B + (k - k^o\cot\Theta'_B)\sin^2\Theta'_B,\\
b =& (k + k^o \cot\Theta_A)\sin\Theta_A\sin\Theta_B,\\
b' =& (k + k^o \cot\Theta_B)\sin\Theta_A\sin\Theta_B,\\
c_1 =& (k - k^o \cot\Theta'_A)\sin\Theta'_A\sin\Theta'_B,\\
c_1' =& (k - k^o \cot\Theta'_B)\sin\Theta'_A\sin\Theta'_B.
\end{aligned} \tag{3.15}$$

The eigen modes for a system of $2N$ sites is determined by the eigenvalue problem

$$-\lambda u = Du, \tag{3.16}$$

where $u = (u_{A,1}, u_{B,1}, u_{A,2}, u_{B,2}, \ldots u_{A,N}, u_{B,N})^T$ and D is called dynamic matrix with entries given by $\{a, a', b, b', c_1, c_1'\}$.

In the quantum theory of solids, the translational symmetry of the system ensures that the eigenstates of the Hamiltonian can also be the eigenstates of translation operator. In the unitary representations of the eigenstates, the irreducible representations of the translation operator are all of one dimension, i.e., the eigenvalue must be $e^{i\frac{2\pi n}{N}}$ under the translation by a unit cell. It leads strong constraints for the form of the wave functions according to Bloch's theorem.

In non-Hermitian system, there is no such unitary requirement. Even in the presence of the translational symmetry (continuous or discrete) for the dynamics matrix, "wave functions" are not necessarily invariant under translation and the momentum or quasi-momentum are not well defined. [1]

[1] A symmetry of the equation of motions is not necessarily the symmetry for its solution. In quantum field theory,

This can be illustrated by a simple ODE as follows.

$$\begin{aligned} &\frac{\mathrm{d}^2}{\mathrm{d}x^2}u = -(\epsilon + \mathrm{i}\gamma)u; \\ &u(x) = A\exp\left(\pm\mathrm{i}\sqrt{(\epsilon+\mathrm{i}\gamma)}x\right). \end{aligned} \tag{3.17}$$

A generic value of the square root in the above equation has a non-vanishing imaginary part, therefore the solution is always exponentially decaying or increasing. It turns out to be a generic feature for the non-Hermitian systems, which is often referred to as non-Hermitian skin effect.

In fact, to solve Eq. 3.16 one has to specify the boundary conditions. We have intensionally organised the terms in a way similar to the usual one dimensional string of coupled oscillators. Since each oscillator is coupled to two neighbours, this is an equation of second order in space (compared to the discretised version of Laplacian), therefore two boundary conditions are needed.

Two intuitive choices of the boundary conditions same as the Hermitian cases are the fixed boundary condition and the periodic boundary condition. In the Hermitian case, the spectrum obtained for the fixed boundary condition and the periodic boundary condition has only small differences. They agree with each other in the thermodynamics limit $N \to \infty$, except for the boundary modes. This is not the case for the non-Hermitian systems. The spectrum for the periodic boundary condition is quite different to that of the fixed boundary condition. In fact the periodic boundary condition requires the solutions to be invariant under the translation by N unit cells, while the solutions to the fixed boundary condition explicitly break the translation symmetry and are all localised exponentially.

Nevertheless, if one only compares the real part of the spectrum, two choices of the boundary conditions have the solutions covering the same intervals. This motivates us to associate these localised modes found in fixed boundary condition still to the "bulk" modes. However, what we mean by "bulk" modes is generalised.

This generalisation can be justified by the transfer matrix in real space formalism. The dynamic matrix in real space in Eq. 3.16 is band diagonal. This allows us to solve $u_{A,n+1}, u_{B,n}$ in terms of

it is known as the spontaneous symmetry breaking. More interestingly, it is pointed out by Polyakov in a lecture of modern classical mechanics that even the solution possesses the symmetry, a local observation within measurement uncertainty may overlook the symmetry. For example, suppose an observable evolves as $O = A\exp(\alpha t) + A\exp(-\alpha t)$, which is invariant under time reversal symmetry. At a time t large enough, one may not be able to resolve the exponentially small part and the time reversal symmetry appears broken.

$u_{A,n}, u_{B,n-1}$.

$$\begin{aligned}
-\lambda u_{A,n} =& + c_1 u_{B,n-1} - a u_{A,n} + b u_{B,n}, \\
-\lambda u_{B,n} =& + b' u_{A,n} - a' u_{B,n} + c_1' u_{A,n+1}; \\
u_{B,n} =& \frac{-(\lambda - a)}{b} u_{A,n} - \frac{c_1}{b} u_{B,n-1}, \\
u_{A,n+1} =& - \frac{b'}{c_1'} u_{A,n} + \frac{-(\lambda - a')}{c_1'} u_{B,n} \\
=& - \frac{b'}{c_1'} u_{A,n} + \frac{(\lambda - a')}{c_1'} \frac{(\lambda - a)}{b} u_{A,n} + \frac{(\lambda - a')}{c_1'} \frac{c_1}{b} u_{B,n-1}.
\end{aligned} \tag{3.18}$$

The third line is obtained directly from the first line. The fourth line is to obtained by manipulating the second line in a similar way, and one substitutes the third line for $u_{B,n}$. The result of Eq. 3.18 may be organised more concisely as

$$\begin{aligned}
\begin{pmatrix} u_{B,n} \\ u_{A,n+1} \end{pmatrix} &= Q_R \begin{pmatrix} u_{B,n-1} \\ u_{A,n} \end{pmatrix}, \\
Q_R &= \begin{pmatrix} -\frac{c_1}{b} & \frac{-(\lambda - a)}{b} \\ \frac{(\lambda - a')}{c_1'} \frac{c_1}{b} & \left[-\frac{b'}{c_1'} + \frac{(\lambda - a')}{c_1'} \frac{(\lambda - a)}{b} \right] \end{pmatrix},
\end{aligned} \tag{3.19}$$

The physical meaning of the matrix Q_R defined above is self-evident, i.e., once the amplitudes of the n-th unit cell $\{u_{A,n}, u_{B,n-1}\}$ is given, the amplitudes of the $(n+1)$-th unit cell $\{u_{A,n+1}, u_{B,n}\}$ is obtained by multiplying the matrix Q_R. In other words, Q_R is nothing but the right transfer matrix.

Instead of the boundary condition problem defined by the dynamic matrix, we now consider the initial value problem defined by the right transfer matrix. It is obvious that two methods are equivalent. The translational symmetry is now also obvious as Q_R is independent n.

Denote $A = bc_1'$,$B = bb' + c_1 c_1' - (a - \lambda)(a' - \lambda)$, $C = b' c_1$, and $\Delta = B^2 - 4AC$. We have the eigenvalues and eigenvectors of Q_R

$$\begin{aligned}
\beta^{(\pm)} =& \frac{1}{2A}(-B \pm \Delta); \\
\xi^{(\pm)} \sim& \begin{pmatrix} B \pm \sqrt{\Delta} \\ 2c_1(\lambda - a') \end{pmatrix} \sim \begin{pmatrix} 2c_1'(\lambda - a) \\ B \pm \sqrt{\Delta} \end{pmatrix}.
\end{aligned} \tag{3.20}$$

Now any solution must be a linear combination of $\xi^{(\pm)}$, i.e.,

$$\begin{pmatrix} u_{B,n} \\ u_{A,n+1} \end{pmatrix} = u_- \left[\beta^{(-)}\right]^n \xi^{(-)} + u_+ \left[\beta^{(+)}\right]^n \xi^{(+)}, \tag{3.21}$$

where $u_\pm$ are constants determined by the initial conditions or the boundary conditions.

Recall that, the bulk modes for fixed boundary condition should be defined as the system size $N \to \infty$. Let N_0 be a finite size cut-off, then we have fixed boundary condition $u_{A,N_0+1} = 0$ at $n = N_0$. In fact, we requires this to be true for arbitrarily large cut-off N_0. This cannot be true unless

$$|\beta^{(+)}| = |\beta^{(-)}| \tag{3.22}$$

This is the bulk mode condition.

In the Hermitian case, $\beta = \exp(\mathrm{i}ka)$. It is not surprising that β is the eigenvalue of the translation operator by a unit cell. In fact the right transfer matrix is a representation of the translation operator. In the non-Hermitian case, this representation is not unitary, therefore the norm of a generic β is not 1. This confirms the existence of the non-Hermitian skin effect.

Now that the bulk modes are defined, we are able to tell if an eigen mode is a bulk mode or an edge mode even though both of then are exponentially localised. Then a natural question will be wether the edge modes (if they exist) are topological? Furthermore, if so, how do we characterise it?

It is well known in the quantum Hall effect, the existence of the chiral edge states is topological. The topological nature is revealed in Ref. [77], where the Hall conductance is associated to the bulk Chern number. In SSH model, it is the Zak phase modulo 2π indicating the topological edge states. Both the Chern number and the Zak phase are obtained by integrating the Berry curvature (2-form) or Berry connection (1-form) over the Brillouin zone.

Nevertheless, the Brillouin zone in the non-Hermitian system is not obviously defined as the quasi-momentum are not well defined. We will show that, instead of the quasimomentum k, the eigenvalue β of the transfer matrix Q can be used for generalising the definition of the Brillouin zone.

Let us come back to the transfer matrix Eq. 3.19 and its solution Eq. 3.21. Although it is equivalent to the eigenvalue problem defined by the dynamic matrix (Eq. 3.18), for more complicated

cases (more sites within a unit cell, couplings to farther neighbours etc.), it is almost impossible to solve explicitly Q_R explicitly. Furthermore this method will also be hard to generalise to higher dimensions. However, It is heuristic to observe that the form of the solution in Eq. 3.21 resembles the Bloch waves. We shall then take this as our ansatz for generalised Bloch waves in non-Hermitian systems

$$\begin{pmatrix} u_{A,n} \\ u_{B,n} \end{pmatrix} = \beta^n \begin{pmatrix} u_A \\ u_B \end{pmatrix}. \tag{3.23}$$

Substitute Eq. 3.23 for the corresponding terms in the equation of motions (Eq. 3.18) we have

$$\begin{aligned} -\lambda u_A &= +c_1\beta^{-1}u_B - au_A + bu_B, \\ -\lambda u_B &= +b'u_A - a'u_B + c_1'\beta u_A; \\ -\lambda \begin{pmatrix} u_A \\ u_B \end{pmatrix} &= D(\beta) \begin{pmatrix} u_A \\ u_B \end{pmatrix}, \\ D(\beta) &= \begin{pmatrix} -a & b + c_1\beta^{-1} \\ b' + c_1'\beta & -a' \end{pmatrix}. \end{aligned} \tag{3.24}$$

This eigenvalue problem has non-trivial solution only when $\det(D(\beta) + \lambda) = 0$, i.e.

$$\begin{aligned} &(\lambda - a)(\lambda - a') - (b + c_1\beta^{-1})(b' + c_1'\beta) = 0, \\ &bc_1'\beta^2 + (bb' + c_1c_1' - (\lambda - a)(\lambda - a'))\beta + b'c_1 = 0. \end{aligned} \tag{3.25}$$

Without surprise we arrive at the same equation for β as the transfer matrix method.

It is worth a remark here that Eq. 3.24 is not just a reproduce of the derivation of the transfer matrix. Since β is a generalisation of $\exp(\mathrm{i}ka)$ for non-Hermitian systems, $D(\beta)$ is an analogy to $H(k)$ in ordinary band theory. We call $D(\beta)$ *reduced dynamic matrix*. In our case, all the allowed β form a loop in complex plane homeomorphic to S^1, although their norm are not 1 in general. This loop now can be considered as a generalised Brillouin zone. Particularly, one may choose $\arg\beta$ as a parameterisation of the generalised Brillouin zone for the non-Hermitian system. By abuse of the notation we will denote $q = \arg\beta$ for convenience. It should be emphasise this q has nothing to do with the quasi-momentum, while its meaning should be evident and unambiguous from the context.

Now we move to the definition of the Zak-Berry phase. In the Hermitian system, one use the

periodic part to define the Berry connection

$$\mathcal{A} = \mathrm{i}\langle u(k)|\mathrm{d}|u(k)\rangle. \tag{3.26}$$

In the non-Hermitian case, this definition of the Berry connection can be formally retained with $\langle u|$ and $|u\rangle$ being left and right eigenvectors of the reduced dynamic matrix $D(\beta)$. This choice is justified by the biorthogonality of the eigenvectors of the non-Hermitian matrix [93]. For a generic non-Hermitian $D(\beta)$ the right eigenvectors are not orthogonal to each other with respect to the canonical Hermitian metric. In the defective limit, two eigenvectors will coalign. [2] However, the left and right eigenvectors associated to the different eigenvalues are canonically orthogonal. The tensor product of a pair of left and right eigenvectors associated to the same eigenvalues can be canonically normalised. (It still leaves an arbitrariness for the normalisation for each individual of them.) Therefore by using left-and right-eigenvector pairs, we have the orthonormality and the completeness, which is important in many derivations of the formulae. This point has been overlooked in Ref. [71].

One defines

$$\gamma = \oint_{\mathcal{C}} A(\beta)\mathrm{d}q_\beta, \tag{3.27}$$

This is a topological indicator. The phase diagram of the 1D rotor chain has been summarised in Fig. 3.6. When $|c_1 c_1'| > |bb'|$, the system is in the topological non-trivial phase. There are topologically protected edge modes. When $|c_1 c_1'| < |bb'|$, the system is in the trivial phase.

3.4 2D Rotor Lattice with Odd Elasticity

In this section, we consider 2D lattice with odd elasticity. Fig. 3.7 shows a unit cell of 2D rotors attached to the honeycomb lattice and connected with the metabeams. The unit cell is defined by vector $\mathbf{a}_{1,2} = \left(\mp\frac{\sqrt{3}}{2}a, \frac{3}{2}a\right)^T$, where a is the edge length of the honeycomb lattice. In each unit cell there are two lattice points which we call A site and B site. The site A (resp. site B) is connected to three site B's (resp. site A's) with three metabeams. The angular positions of the rotors (specified by the tangential vectors) are denoted as $\theta_{A,B}$, and the angular positions of the metabeams are

[2] In our case, the defective case will not bother us as it always has two degenerate eigenvalues. As we assume the spectrum of our system should always have a gap, the defective case is excluded. Nevertheless, when one tries to generalise the Dirac/Weyl semimetals to the non-Hermitian correspondence, defective point can be a way two band touches. This will be an interesting question for future researches beyond the current thesis.

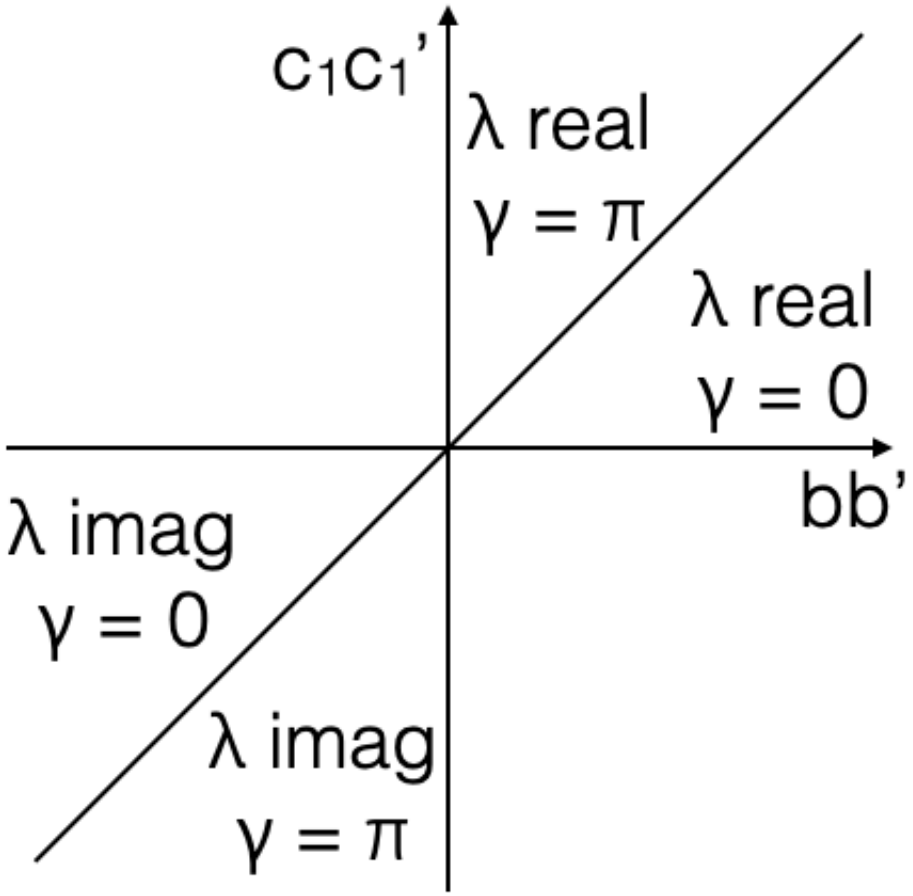

Figure 3.6: Phase diagram of 1D rotor chain.

denoted as $\theta_i, i = 1, 2, 3$. All the angles are measured with respect to the x-axis. To simplify the notations, we denote $\Theta_{Ai} = \theta_A - \theta_i$ and $\Theta_{Bi} = \theta_B - \theta_i$. Then, we have the equations of motion linearised near equilibrium position

$$\begin{aligned} m\ddot{u}_{A,n_1n_2} =& + c_1 u_{B,(n_1-1)n_2} + c_2 u_{B,n_1(n_2-1)} - a u_{A,n_1n_2} + b u_{B,n_1n_2}, \\ m\ddot{u}_{B,n_1n_2} =& + b' u_{A,n_1n_2} - a' u_{B,n_1n_2} + c_1' u_{A,(n_1+1)n_2} + c_2' u_{A,n_1(n_2+1)}, \end{aligned} \tag{3.28}$$

where the parameters are given by

$$\begin{aligned} a =& \sum_{i=1,2,3} (k + k^o \tan\Theta_{Ai}) \cos^2\Theta_{Ai}, \\ a' =& \sum_{i=1,2,3} (k + k^o \tan\Theta_{Bi}) \cos^2\Theta_{Bi}, \\ b =& (k + k^o \tan\Theta_{A3}) \cos\Theta_{A3} \cos\Theta_{B3}, \\ b' =& (k + k^o \tan\Theta_{B3}) \cos\Theta_{B3} \cos\Theta_{A3}, \\ c_1 =& (k + k^o \tan\Theta_{A1}) \cos\Theta_{A1} \cos\Theta_{B1}, \\ c_1' =& (k + k^o \tan\Theta_{B1}) \cos\Theta_{B1} \cos\Theta_{A1}, \\ c_2 =& (k + k^o \tan\Theta_{A2}) \cos\Theta_{A2} \cos\Theta_{B2}, \\ c_2' =& (k + k^o \tan\Theta_{B2}) \cos\Theta_{B2} \cos\Theta_{A2}. \end{aligned} \tag{3.29}$$

As we have seen in Sec. 3.3, the spectrum of the non-Hermitian system is sensitive to the boundary conditions. We will only discuss the fixed boundary conditions, i.e., the amplitudes of the sites on the boundaries vanish.

Fig. 3.8 shows a typical bulk mode (left panel) and a typical edge mode (right panel). The markers have their size proportional to the amplitude. The left panel shows a mode that would be symmetric with respect to the diagonals of the rhombus in the absence of the odd elasticity. Nevertheless, it is obvious that the weight of the mode is heavier in the lower half rhombus, which is a manifestation of the non-Hermitian skin effect. In fact, the non-Hermitian skin effect exists no matter the system is in the topologically non-trivial phase or in the topologically trivial phase. Fig. 3.9 shows a (bulk) mode similar to the bulk mode in the left panel of Fig. 3.8 but in a topologically trivial phase.

It is interesting to observe that the edge modes reside only on the upper right edge and the bottom left edge but not on the other two edges. It is in contrast to the quantum Hall effect (Haldane model), where the topological edge modes are chiral modes localised on all four edges and forming a closed loop. It turns out that the topological edge modes are still characterised by some

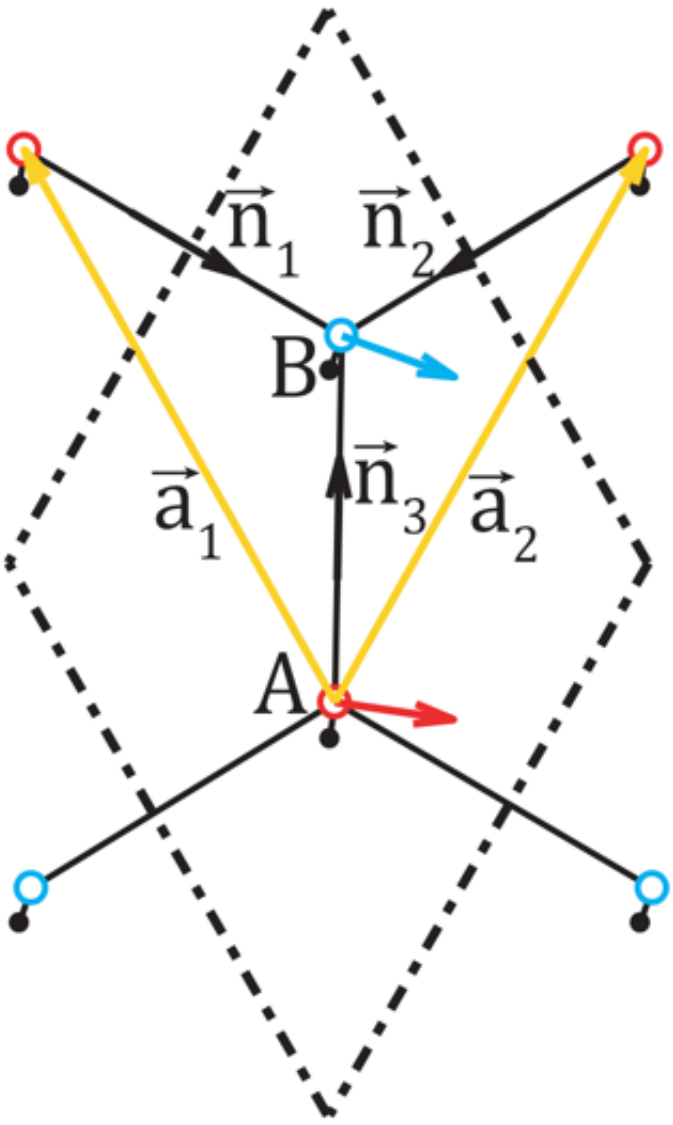

Figure 3.7: Unit cell of 2D rotor lattice.

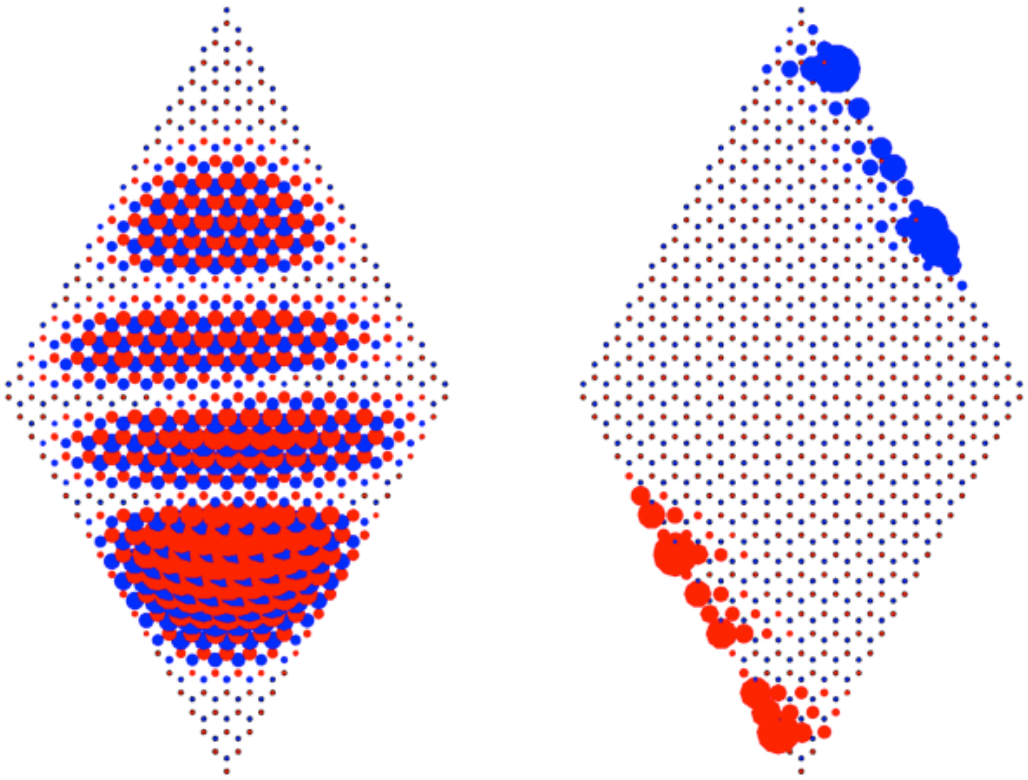

Figure 3.8: A bulk mode and an edge mode of 2D rotor lattice in topological non-trivial phase.

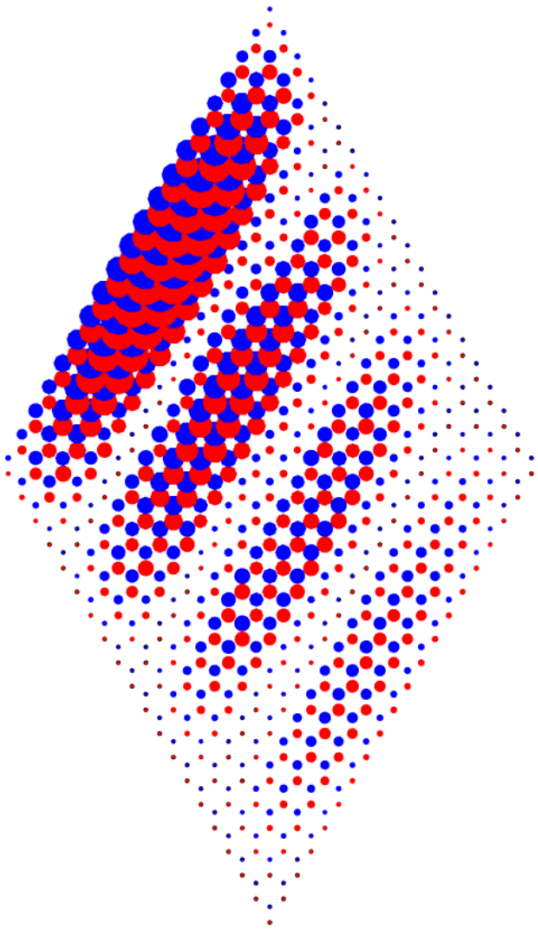

Figure 3.9: A bulk mode of 2D rotor lattice in topological trivial phase.

winding number as a generalisation of the one we defined in Sec. 3.3. A closer analogy in the electron systems can be the polarisation model of King-Smith and Vanderbilt [35].

More quantitatively, we use the ansatz of the generalised Bloch wave

$$\begin{pmatrix} u_{A,n_1n_2} \\ u_{B,n_1n_2} \end{pmatrix} = \mathrm{e}^{-\mathrm{i}\omega t}\beta_2^{n_2}\beta_1^{n_1}\begin{pmatrix} u_A \\ u_B \end{pmatrix}. \tag{3.30}$$

It transforms the equations of motion to an eigenvalue problem for a 2-by-2 dynamical matrix

$$D(\beta_1,\beta_2) = \begin{pmatrix} a & -(b+c_1\beta_1^{-1}+c_2\beta_2^{-1}) \\ -(b'+c_1'\beta_1+c_2'\beta_2) & a' \end{pmatrix} \tag{3.31}$$

For a given β_2, we may solve β_1 from the eigenvalue problem

$$\beta_1^{(\pm)} = \frac{1}{2A}(-B \pm \sqrt{\Delta}), \tag{3.32}$$

where

$$\begin{aligned} \lambda =& m\omega^2, \\ A =& bc_1' + c_1'c_2\beta_2^{-1}, \\ B =& bb' + c_1c_1' + c_2c_2' + bc_2'\beta_2 + b'c_2\beta_2^{-1} - (a-\lambda)(a'-\lambda), \\ C =& b'c_1 + c_1c_2'\beta_2, \\ \Delta =& B^2 - 4AC. \end{aligned} \tag{3.33}$$

A bulk mode means $|\beta_1^{(+)}| = |\beta_1^{(-)}|$, i.e., Eq. 3.32 gives a pair of conjugate β_1, or equivalently AC/B^2 being real as well as $\Delta < 0$. From these conditions we solve the norm of β_2

$$|\beta_2| = \sqrt{\frac{b'c_2}{bc_2'}}, bb'c_2c_2' > 0. \tag{3.34}$$

Reciprocally, we also have the norm of β_1

$$|\beta_1| = \sqrt{\frac{b'c_1}{bc_1'}}, bb'c_1c_1' > 0. \tag{3.35}$$

The norms of β_1 and β_2 are not unital in general, which describes localisation of the bulk modes due to the non-Hermitian skin effect.

We define the Berry phases γ_i along each direction of the base vector $\mathbf{a}_i$

$$\begin{aligned}\gamma_1(\beta_2) =& \oint_{\mathcal{C}_i} \mathcal{A}_1(\beta_1,\beta_2)\mathrm{d}q_{\beta_1},\\ \gamma_2(\beta_1) =& \oint_{\mathcal{C}_i} \mathcal{A}_2(\beta_1,\beta_2)\mathrm{d}q_{\beta_2},\\ \mathcal{A}_i(\{\beta_i\}) =& \mathrm{i}\langle u^{(L)}(\beta_i,\beta_2)|\partial_{q_{\beta_i}}|u^{(R)}(\beta_i,\beta_2)\rangle.\end{aligned} \tag{3.36}$$

where $\mathcal{C}_i$ is the fundamental loop in the generalised Brillouin zone parameterised by the argument of β_i. In Eq. 3.36, the dependence of γ_1 on β_2 and the dependence of γ_2 on β_1 has been made explicit. In contrast to the 1D case, the Berry phase so defined is not integral multiples of π for all generic β_i in the generalised Brillouin zone. Similar to the 1D case, we have a symmetry transformation $\mathcal{I}D(\beta_i)\mathcal{I}^{-1} = D(\beta_i^*)$. Therefore, $\gamma_1(\beta_2) = -\gamma_1(\beta_2^*)(\mod 2\pi)$ and $\gamma_1(\beta_2) = -\gamma_1(\beta_2^*)(\mod 2\pi)$. If we average the Zak-Berry phase, we have

$$\begin{aligned}\gamma_1 =& \frac{1}{2\pi}\int_{-\pi}^{\pi} \gamma_1(\beta_2)\mathrm{d}q_{\beta_2},\\ \gamma_2 =& \frac{1}{2\pi}\int_{-\pi}^{\pi} \gamma_2(\beta_1)\mathrm{d}q_{\beta_1},\end{aligned} \tag{3.37}$$

being integral multiples of π. These are topological indicators of the topological edge modes. In the Hermitian case, the symmetry $\mathcal{I}$ has a simple physical interpretation, i.e., the inversion symmetry.

Fig. 3.10 summarieses the phase diagram of the 2D rotor lattice. When $(\gamma_1,\gamma_2) = (\pi,0)$, the topological edge modes are localised on the upper-left edge and bottom-right edge; when $(\gamma_1,\gamma_2) = (0,\pi)$, the topological edge modes are localised on the upper-right edge and bottom-rleft edge. When $(\gamma_1,\gamma_2) = (0,0)$, the system is topologically trivial, and there are no topological edge modes. (But the bulk modes also have exponential envelope profile due to the non-Hermitian skin effect.) There is a region in the parameter space where the spectrum is not separable.

3.5 Conclusion and Discussion

We discussed 1D rotor chain and 2D rotor lattice connected by metabeams with odd elasticity. The system is described by some non-Hermitian dynamic matrix D. In analogy to the SSH model, there exist topological modes in these systems. In order to characterise the topological modes, we associate the bulk modes to the generalised Brillouin zone. The definition of the Zak-Berry phase has been clarified in biorthogonal Bloch vectors. The Zak-Berry phase can be used as topological indicators for the topological modes, which is a generalisation of the bulk-boundary correspondence to the

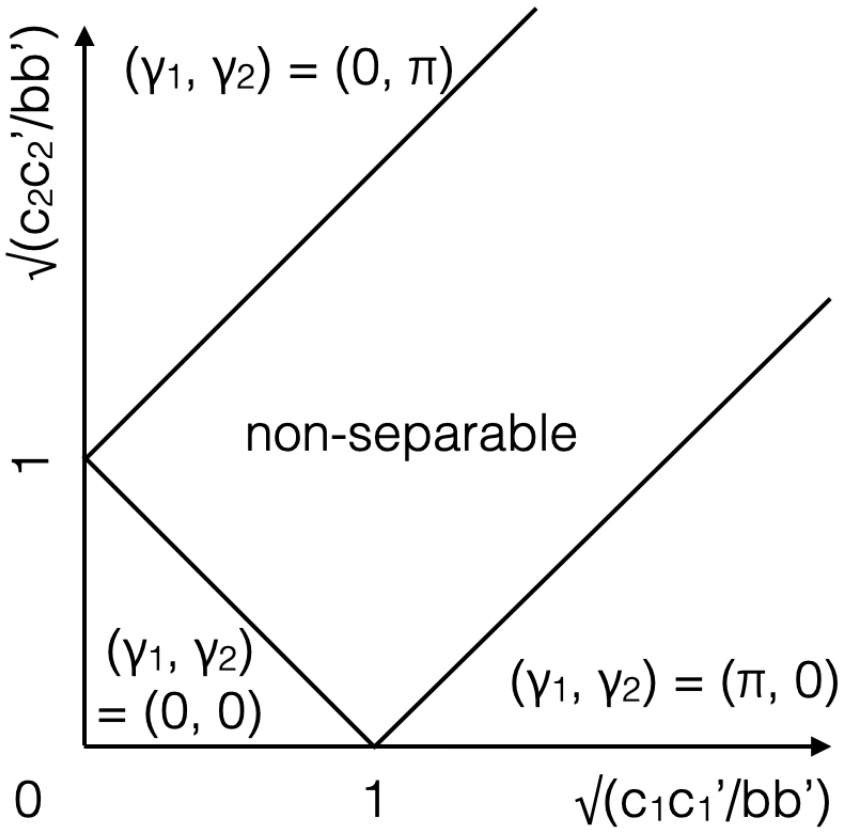

Figure 3.10: Phase diagram of 2D rotor lattice.

non-Hermitian system. As a generic feature, even in the presence of the translational symmetry, the transfer matrix does not have unital eigenvalues, therefore even the bulk modes are also localised exponentially, which is known as non-Hermitian skin effect.

In Ref. [93], we also discussed 2D honeycomb lattice, where the mass points are free from the rotor constraints. It turns out the non-Hermitian skin effect is absent in the 2D honeycomb lattice even if the metabeams have non-vanishing odd elasticity.

Chapter 4

Outlook

In this thesis, two idealised models have been studied. Both of them were motivated by some biochemical systems. Concepts of topology and phase transition have been applied to the models, while extensions are also needed to accommodate new features compared to the conventional electronic systems. The non-Hermitian dynamics arise from the odd elasticity can only be realised in the systems with active energy pumping. In general, more complicated dynamics can arise in active matter, e.g., systems driven far from equilibrium, and non-linear effect. New types of topological phase transition have also been found arising due to the non-linearity [92].

The models discussed in this thesis are just like a drop of water in the ocean of the condensed matter physics, whereas one tries to peek the world through the droplet. A system is considered well understood if one can make predictions of the system based on simple principles, which forms a paradigm of epistemology of the natural philosophy or the natural sciences. On the other hand, even though we know the physical fundamentals, understanding complicated phenomena emerging at multiple scales is still beyond our current scope. Protein folding problem i is such a problem remaining open. Deep learning sheds a light on this problem thanks to the development of the computation power over the past four score years. Yet it does not provide a satisfactory understanding from physics point of view. Within the expectable future, quantum computation will even boost our computation power. It provides a revolutionary tool to explore the complicated systems from bottom up. Perhaps as entropy and temperature is to the statistical physics versus the classical mechanics, with the inflation of the data scale and computation power, revolutionary new concepts may be also needed.

Chapter 5

Appendices

5.1 Lee-Yang Lattice Gas

Lee and Yang had a heuristic and insightful view on the phase transition. In Ref. [85] and Ref. [46], they considered the zero points of the partition function for complex fugacity. In Ref. [46], a lattice gas model was mapped to an Ising model. Therefore, properties of the liquid-gas phase transition may be tracked with the help of the knowledge of the Ising model. The model in Chap. 2 was also motivated by a similar spirit. In this section of the Appendices, we shall transcribe the correspondence of the lattice gas model and the Ising model in Ref. [46] with a notation consistent in this thesis.

Consider lattice gas consisting of monomers occupying vertices of a lattice $L = \{V, E\}$. The monomers have hard-core repulsion, therefore two monomers are not allowed to occupy the same vertex site. If one also consider the nearest neighbour interaction, i.e., two monomers attract each other with a potential energy u if they sit on nearest neighbouring sites.

Instead of focusing on the monomers, one may regard the occupation of the lattice L. Therefore, one may define an occupation function

$$Q(v) = \begin{cases} +1, & \text{if } v \text{ is occupied by a monomer,} \\ 0, & \text{if } v \text{ is empty.} \end{cases} \tag{5.1}$$

Then the density of the gas is

$$n = \frac{1}{|V|} \sum_{v \in V} Q(v). \tag{5.2}$$

The nearest neighbour interaction u can be mapped to an Ising model with ferromagnetic couplings if $u < 0$ or with antiferromagnetic couplings if $u > 0$. Let spin up represents empty site and spin down represent occupied site. The spin configuration is related to the occupation function as

$$S(v) = \frac{1}{2} - Q, \tag{5.3}$$

where we have normalised spins to $\frac{1}{2}$. The order parameter (magnetisation) of the ferromagnetic Ising model is

$$M = \frac{1}{|V|} \sum_{v \in V} S(v). \tag{5.4}$$

So $M = \frac{1}{2} - n$.

The Hamiltonian of the lattice gas can be transcribed by the occupation function

$$H_Q = \sum_{v_1, v2 \in \partial e}^{e \in E_{nn}} uQ(v_1(e))Q(v_2(e)). \tag{5.5}$$

In terms of Ising model we have equivalently

$$H_{nn} = \sum_{v_1, v2 \in \partial e}^{e \in E_{nn}} uS(v_1(e))S(v_2(e)) - \frac{1}{2} \sum_{v \in V} uz_{nn}(v)S(v) + \frac{1}{4}u|E_{nn}|, \tag{5.6}$$

where $z_{nn}(v)$ is the nearest neighbour coordination number of vertex v. In addition to the nearest neighbour interaction, there is also a chemical potential term $-\mu N = -\mu \sum_{v \in V} Q(v)$ in the lattice gas model, which is equivalent to $H_\mu = \mu \sum_{v \in V} S(v) - \frac{1}{2}\mu|V|$.

So up to an additive constant, the Ising model associated to the lattice gas model is described by the Hamiltonian

$$H_{\text{Ising}} = -J \sum_{v_1, v2 \in \partial e}^{e \in E_{nn}} S(v_1(e))S(v_2(e)) - h \sum_{v \in V} S(v), \tag{5.7}$$

where $J = -u$ and $h = \frac{1}{2}uz_{nn} - \mu$.

5.2 Ising Models

In this section, results of the Ising model used in this thesis is summarised.

Peierls contour argument is useful for proving the existence of a phase transition. We follows

Ref. [3] for the Peierls contour argument. Consider an Ising model with the cost of a single bond excitation being $2J$. Let γ be a contour on a lattice L such that the spins in the interior region and the spins in the exterior region take constant values but with opposite sign. The probability of contour γ in terms of the Gibbs measure has an upper bound

$$\begin{aligned} P(\gamma) =& \frac{\sum_{\{\sigma\}\in\Sigma} \mathbb{1}_\gamma(\{\sigma\}) \exp[-\beta H_I(\{\sigma\})]}{\sum_{\{\sigma\}\in\Sigma} \exp[-\beta H_I(\{\sigma\})]} \\ \leq& \frac{\sum_{\{\sigma\}\in\Sigma} \mathbb{1}_\gamma(\{\sigma\}) \exp[-\beta H_I(\{\sigma\})]}{\sum_{\{\sigma\}\in\Sigma} \mathbb{1}_\gamma(\{\sigma\}) \exp[-\beta H_I(T\{\sigma\})]} = \mathrm{e}^{-\beta(2J|\gamma|)}, \end{aligned} \tag{5.8}$$

where $|\gamma|$ is the length of the contour, and $\mathbb{1}_\gamma(\{\sigma\})$ is the indicator function of appearance of γ on the spin configuration space. In the second step of the inequality, we retain a subset of the sum in the denominator, where the spin configuration $T\{\sigma\}$ is obtained by flipping the spins in the interior of γ. Then, there there is a one-to-one correspondence for the terms in the numerator and in the denominator, while each term in the denominator gains an energy of $2J|\gamma|$ over the corresponding term in the numerator due to the elimination of the domain wall γ.

Let us assume that on the boundary of the lattice, all the spins are pointing upwards. We would estimate the probability of a spin on a generic site $v \in L$ far from the boundary pointing downwards. In order that such event can happen, it is necessary to have a contour γ encircling v. Therefore, the probability $P(\sigma(v) = \downarrow)$ has an upper bound

$$\begin{aligned} P(\sigma(v) = \downarrow) \leq& \sum_{\gamma: v\in\mathring{D}_\gamma} P(\gamma) \\ =& \sum_{l\geq l_0} \mathcal{N}[\gamma | v \in \mathring{D}_\gamma, |\gamma| = l] \mathrm{e}^{-\beta(2Jl)} \\ \leq& \sum_{l\geq l_0} l^2 z_{nn}^l \mathrm{e}^{-\beta(2Jl)} \end{aligned} \tag{5.9}$$

where $\mathcal{N}[\gamma | v \in \mathring{D}_\gamma, |\gamma| = l]$ counts the number of contours of length l such that v is in the interior region $\mathring{D}_\gamma$. The sum in the last line is uniformly controlled by the exponential function. So, there exists a large enough but finite β such that the probability $P(\sigma(v) = \downarrow) < \frac{1}{2}$, which means the average magnetisation does not vanish.

The estimations in Eq. 5.8 and Eq. 5.9 are definitely not optimal. The inequality in Eq. 5.8 is due to numerous terms discarded for the sum in the denominator. The first inequality in Eq. 5.9 comes from the necessary but not sufficient condition of existence of γ encircling v. The counting in the last step is very loose without taking detail conditions of the γ into account. It can be improved e.g.,

by counting only self-avoiding loops, which can be quite involved. Because of these disadvantages, the Peierls contour argument is often useful to demonstrate the existence of the phase transition but hard to be used for estimating the critical temperature.

In spite of Onsager's ingeneous solution of the Ising model [57], Kramers and Wannier obtained the critical temperature with the duality argument [40] before Onsager's solution. Intuitively, the duality may be understood as a correspondence of the terms in the low temperature expansion and the high temperature expansion of the partition function. In the low temperature expansion, contours encircling excited spins as domain walls, which is similar to what we described in Peierls contour argument. At high temperature

$$\begin{aligned} Z &= \sum_{\{\sigma\}\in\Sigma} \exp[-\beta H(\{\sigma\})] = \sum_{\{\sigma\}\in\Sigma} \prod_{e\in E} \exp[\beta J\sigma(v_1(e))\sigma(v_2(e))] \\ &= \sum_{\{\sigma\}\in\Sigma} \prod_{e\in E} [1+\beta J\sigma(v_1(e))\sigma(v_2(e)) + \dots]. \end{aligned} \tag{5.10}$$

For each σ, the sum is taken positive value and negative value symmetrically. Therefore, terms in the expansion of the product with odd number of some spin σ does bot contribute to the partition function. Then, the leading terms in the high temperature expansion are the terms with edges forming loops.

Onsager obtained the critical temperature of 2D Ising model on square lattice with anisotropic couplings determined by

$$\sinh(2\beta_c J_\parallel)\sinh(2\beta_c J_\perp) = 1. \tag{5.11}$$

It is hard to understand Onsager's algebraic method even with subsequent simplifications [33, 84].

An alternative way to solve the Ising model was given by Schultz, Mattis, and Lieb based on transfer matrix [69]. They mapped the Ising model to free fermions. At the critical temperature, the mass gap of the fermions vanishes and the conformal symmetry emerges. In 3D, an exact solution like the one obtained by Onsager seems hopeless, while the conformal symmetry at the critical point may help understand the phase transition and extract the critical exponents [66].

Another variant of the Ising model was considered by Kazakov [34]. One consider the following action for the two matrix model

$$S = \mathrm{Tr}(U^2 + V^2 - 2cUV + \frac{g}{n}(U^4 + V^4)), \tag{5.12}$$

where $c = \exp(-2\beta J)$ in our notation. Perturbative expansion leads to the diagrams consist of vertices of degree 4. When the rank of the matrices $N \to \infty$, only the planar diagrams retains. On the other hand, $n \to \infty$ corresponds to the thermal dynamic limit, i.e., the diagrams with infinite vertices. In this representation, two spin states are associated to two species of matrices on the vertices. A single critical point is obtained at $c = \frac{1}{4}$, therefore $k_B T_c = \frac{J}{\ln 2}$.

5.3 List of Other Published or Unpublished Works

[1] H. Zheng, **JYZ**, and R. Berndt, A Minimal Double Quantum Dot, *Sci. Rep.*, **7**, 10764 (2017).

Double quantum dots formed by neighbouring doping atoms in ZnO is studied by STM/STS (scanning tunnelling microscopy/scanning tunnelling spectroscopy). I proposed a model of interacting electrons for understanding the system. I calculated the charge stability diagram which agrees well with the measurement of STM/STS. I also discussed about potential applications for preparing entangled pairs with coherent microwave driving.

[2] **JYZ** and F. D. M. Haldane, Surface corrections to the chiral anomaly in the Weyl semimetals, unpublished

Chiral anomaly in the Weyl semimetals may lead to negative magnetoresistance. Surface corrections caused by the Fermi arcs has been discussed.

[3] **JYZ** and F. D. M. Haldane, Landau levels on constantly curved space, unpublished

An algebraic method to solve the Landau levels on hyperbolic plane has been worked out. The Landau level raising and lowering operators $A^\dagger$ and A have been constructed explicitly. The spectrum can be obtained according to the modified oscillator algebra generated by $A^\dagger$ and A.

[4] **JYZ**, EIT-Enhanced Coupled-Resonance Spectroscopy, arXiv:1707.09559

An improvement by using the EIT effect to enhance the signal of the coupled-resonance spectroscopy has been proposed. A scheme for locking two lasers of different wave lengths to the same atomic source has been designed.

[5] **JYZ**, Testing Case Number of Coronavirus Disease 2019 in China with Newcomb-Benford Law, arXiv:2002.05695 [physics.soc-ph]

A criterion of detecting frauds based Newcomb-Benford Law has been applied to the reported data of COVID19 from China. It indicates a high confidence of no detection of frauds.

Bibliography

[1] J. L. F. Abascal and C. Vega. A general purpose model for the condensed phases of water: Tip4p/2005. *The Journal of Chemical Physics*, 123(23):234505, 2005.

[2] Ian Affleck, Tom Kennedy, Elliott H. Lieb, and Hal Tasaki. Rigorous results on valence-bond ground states in antiferromagnets. *Phys. Rev. Lett.*, 59:799–802, Aug 1987.

[3] Michael Aizenman. *Class notes of MAT521 (Spring 2020).* 2020.

[4] Fabien Alet, Jesper Lykke Jacobsen, Grégoire Misguich, Vincent Pasquier, Frédéric Mila, and Matthias Troyer. Interacting classical dimers on the square lattice. *Phys. Rev. Lett.*, 94:235702, Jun 2005.

[5] G. Algara-Siller, O. Lehtinen, F. C. Wang, R. R. Nair, U. Kaiser, H. A. Wu, A. K. Geim, and I. V. Grigorieva. Square ice in graphene nanocapillaries. *Nature*, 519(7544):443–445, 2015.

[6] P. W. Anderson. More is different. *Science*, 177(4047):393–396, 1972.

[7] J. E. Avron, R. Seiler, and P. G. Zograf. Viscosity of quantum hall fluids. *Phys. Rev. Lett.*, 75:697–700, Jul 1995.

[8] Berezinskii. Destruction of long-range order in one-dimensional and two-dimensional systems having a continuous symmetry group i. classical systems. *Sov. Phys. JETP*, 32:493, 1971.

[9] Berezinskii. Destruction of long-range order in one-dimensional and two-dimensional systems having a continuous symmetry group ii. quantum systems. *Sov. Phys. JETP*, 34:610, 1972.

[10] William Bialek, Andrea Cavagna, Irene Giardina, Thierry Mora, Edmondo Silvestri, Massimiliano Viale, and Aleksandra M. Walczak. Statistical mechanics for natural flocks of birds. *Proceedings of the National Academy of Sciences*, 109(13):4786–4791, 2012.

[11] T. Buckmaster and V. Vicol. Nonuniqueness of weak solutions to the navier-stokes equation. *Ann Math*, 189:101, 2019.

[12] Tristan Buckmaster, Camillo De Lellis, and László Székelyhidi Jr. Dissipative euler flows with onsager-critical spatial regularity. *Communications on Pure and Applied Mathematics*, 69(9):1613–1670, 2016.

[13] Peter Constantin, Weinan E, and Edriss S. Titi. Onsager's conjecture on the energy conservation for solutions of Euler's equation. *Communications in Mathematical Physics*, 165(1):207 – 209, 1994.

[14] Pablo G. Debenedetti, Francesco Sciortino, and Gül H. Zerze. Second critical point in two realistic models of water. *Science*, 369(6501):289–292, 2020.

[15] Lior Ella, Asaf Rozen, John Birkbeck, Moshe Ben-Shalom, David Perello, Johanna Zultak, Takashi Taniguchi, Kenji Watanabe, Andre K. Geim, Shahal Ilani, and Joseph A. Sulpizio. Simultaneous voltage and current density imaging of flowing electrons in two dimensions. *Nature Nanotechnology*, 14(5):480–487, 2019.

[16] John Jumper *et al.* High accuracy protein structure prediction using deep learning. *Fourteenth Critical Assessment of Techniques for Protein Structure Prediction*, page 22, 2020.

[17] Gregory L. Eyink. Energy dissipation without viscosity in ideal hydrodynamics i. fourier analysis and local energy transfer. *Physica D: Nonlinear Phenomena*, 78(3):222–240, 1994.

[18] Charles Fefferman. *Class notes of MAT529 (Fall 2017).* 2017. notes taken by Junyi Zhang.

[19] Nigel Goldenfeld. Roughness-induced critical phenomena in a turbulent flow. *Phys. Rev. Lett.*, 96:044503, Jan 2006.

[20] F. D. M. Haldane. Nonlinear field theory of large-spin heisenberg antiferromagnets: Semi-classically quantized solitons of the one-dimensional easy-axis néel state. *Phys. Rev. Lett.*, 50:1153–1156, Apr 1983.

[21] F. D. M. Haldane. Model for a quantum hall effect without landau levels: Condensed-matter realization of the "parity anomaly". *Phys. Rev. Lett.*, 61:2015–2018, Oct 1988.

[22] F. D. M. Haldane and S. Raghu. Possible realization of directional optical waveguides in photonic crystals with broken time-reversal symmetry. *Phys. Rev. Lett.*, 100:013904, Jan 2008.

[23] B. I. Halperin. Quantized hall conductance, current-carrying edge states, and the existence of extended states in a two-dimensional disordered potential. *Phys. Rev. B*, 25:2185–2190, Feb 1982.

[24] Nora Hassan, Streit Cunningham, Martin Mourigal, Elena I. Zhilyaeva, Svetlana A. Torunova, Rimma N. Lyubovskaya, John A. Schlueter, and Natalia Drichko. Evidence for a quantum dipole liquid state in an organic quasi–two-dimensional material. *Science*, 360(6393):1101–1104, 2018.

[25] Ole J. Heilmann and Elliott H. Lieb. Monomers and dimers. *Phys. Rev. Lett.*, 24:1412–1414, Jun 1970.

[26] Ole J. Heilmann and Elliott H. Lieb. Lattice models for liquid crystals. *Journal of Statistical Physics*, 20(6):679–693, 1979.

[27] John P. Heller. An unmixing demonstration. *Am. J. Phys.*, 28:348, 1960.

[28] Hong-Ye Hu, Shuo-Hui Li, Lei Wang, and Yi-Zhuang You. Machine learning holographic mapping by neural network renormalization group. *Phys. Rev. Research*, 2:023369, Jun 2020.

[29] Phillip Isett. A proof of onsager's conjecture. *Ann Math*, 188:871, 2018.

[30] Gregor Jotzu, Michael Messer, Rémi Desbuquois, Martin Lebrat, Thomas Uehlinger, Daniel Greif, and Tilman Esslinger. Experimental realization of the topological haldane model with ultracold fermions. *Nature*, 515(7526):237–240, 2014.

[31] C. L. Kane and T. C. Lubensky. Topological boundary modes in isostatic lattices. *Nature Physics*, 10(1):39–45, 2014.

[32] C. L. Kane and E. J. Mele. Quantum spin hall effect in graphene. *Phys. Rev. Lett.*, 95:226801, Nov 2005.

[33] Bruria Kaufman. Crystal statistics. ii. partition function evaluated by spinor analysis. *Phys. Rev.*, 76:1232–1243, Oct 1949.

[34] V. A. Kazakov. Ising model on a dynamical planar random lattice: Exact solution. *Physics Letters A*, 119(3):140–144, 1986.

[35] R. D. King-Smith and David Vanderbilt. Theory of polarization of crystalline solids. *Phys. Rev. B*, 47:1651–1654, Jan 1993.

[36] A. Yu. Kitaev. Fault-tolerant quantum computation by anyons. *Annals of Physics*, 303(1):2–30, 2003.

[37] K. v. Klitzing, G. Dorda, and M. Pepper. New method for high-accuracy determination of the fine-structure constant based on quantized hall resistance. *Phys. Rev. Lett.*, 45:494–497, Aug 1980.

[38] Markus König, Steffen Wiedmann, Christoph Brüne, Andreas Roth, Hartmut Buhmann, Laurens W. Molenkamp, Xiao-Liang Qi, and Shou-Cheng Zhang. Quantum spin hall insulator state in hgte quantum wells. *Science*, 318(5851):766–770, 2007.

[39] J. M. Kosterlitz and D. J. Thouless. Ordering, metastability and phase transitions in two-dimensional systems. *Journal of Physics C: Solid State Physics*, 6:1181, 1973.

[40] H. A. Kramers and G. H. Wannier. Statistics of the two-dimensional ferromagnet. part i. *Phys. Rev.*, 60:252–262, Aug 1941.

[41] Flore K. Kunst, Elisabet Edvardsson, Jan Carl Budich, and Emil J. Bergholtz. Biorthogonal bulk-boundary correspondence in non-hermitian systems. *Phys. Rev. Lett.*, 121:026808, Jul 2018.

[42] L. D. Landau and E. M. Lifshitz. *Course of Theoretical Physics, Volume 5: Statistical Physics.* Addison-Wesley, 1969.

[43] L. D. Landau and E. M. Lifshitz. *Course of Theoretical Physics, Volume 7: Theory of Elasticity, 3rd Ed.* Pergamon Press, 1986.

[44] L. D. Landau and E. M. Lifshitz. *Course of Theoretical Physics, Volume 6: Fluid Mechanics, 2nd Ed.* Pergamon Press, 1987.

[45] J. L. Lebowitz and G. Gallavotti. Phase transitions in binary lattice gases. *Journal of Mathematical Physics*, 12(7):1129–1133, 1971.

[46] T. D. Lee and C. N. Yang. Statistical theory of equations of state and phase transitions. ii. lattice gas and ising model. *Phys. Rev.*, 87:410–419, Aug 1952.

[47] Elliott H. Lieb. Residual entropy of square ice. *Phys. Rev.*, 162:162–172, Oct 1967.

[48] Elliott H. Lieb. Solution of the dimer problem by the transfer matrix method. *Journal of Mathematical Physics*, 8(12):2339–2341, 1967.

[49] Elliott H. Lieb. Two theorems on the hubbard model. *Phys. Rev. Lett.*, 62:1201–1204, Mar 1989.

[50] Elliott H. Lieb. Two theorems on the hubbard model. *Phys. Rev. Lett.*, 62:1927–1927, Apr 1989.

[51] Elliott H. Lieb. private communication. 2018.

[52] Chia-Chiao Lin. *Statistical Theories of Turbulence*. Princeton University Press, 1959.

[53] R. Moessner and K. S. Raman. Quantum dimer models. *arXiv:0809.3051v1 [cond-mat.str-el]*, 2008.

[54] R. Moessner and S. L. Sondhi. Resonating valence bond phase in the triangular lattice quantum dimer model. *Phys. Rev. Lett.*, 86:1881–1884, Feb 2001.

[55] Shuichi Murakami, Naoto Nagaosa, and Shou-Cheng Zhang. Dissipationless quantum spin current at room temperature. *Science*, 301(5638):1348–1351, 2003.

[56] L. Onsager. Statistical hydrodynamics. *Il Nuovo Cimento*, 6:279, 1949.

[57] Lars Onsager. Crystal statistics. i. a two-dimensional model with an order-disorder transition. *Phys. Rev.*, 65:117–149, Feb 1944.

[58] Linus Pauling. The structure and entropy of ice and of other crystals with some randomness of atomic arrangement. *Journal of the American Chemical Society*, 57(12):2680–2684, 12 1935.

[59] Alexander Markovich Polyakov. *Class notes of PHY408 (Spring 2016)*. 2016. notes taken by Junyi Zhang.

[60] Songyang Pu, Mikael Fremling, and J. K. Jain. Hall viscosity of composite fermions. *Phys. Rev. Research*, 2:013139, Feb 2020.

[61] S. Raghu and F. D. M. Haldane. Analogs of quantum-hall-effect edge states in photonic crystals. *Phys. Rev. A*, 78:033834, Sep 2008.

[62] N. Read and E. H. Rezayi. Hall viscosity, orbital spin, and geometry: Paired superfluids and quantum hall systems. *Phys. Rev. B*, 84:085316, Aug 2011.

[63] N. Read and E. H. Rezayi. Publisher's note: Hall viscosity, orbital spin, and geometry: Paired superfluids and quantum hall systems [phys. rev. b 84, 085316 (2011)]. *Phys. Rev. B*, 84:119902, Sep 2011.

[64] Daniel S. Rokhsar and Steven A. Kivelson. Superconductivity and the quantum hard-core dimer gas. *Phys. Rev. Lett.*, 61:2376–2379, Nov 1988.

[65] David Ruelle. Existence of a phase transition in a continuous classical system. *Phys. Rev. Lett.*, 27:1040–1041, Oct 1971.

[66] S. Rychkov. 3d ising model: a view from the conformal bootstrap island. *Comptes Rendus. Physique*, 21:185, 2020.

[67] Colin Scheibner, Anton Souslov, Debarghya Banerjee, Piotr Surówka, William T. M. Irvine, and Vincenzo Vitelli. Odd elasticity. *Nature Physics*, 16(4):475–480, 2020.

[68] Nathan Schine, Albert Ryou, Andrey Gromov, Ariel Sommer, and Jonathan Simon. Synthetic landau levels for photons. *Nature*, 534(7609):671–675, 2016.

[69] T. D. SCHULTZ, D. C. MATTIS, and E. H. LIEB. Two-dimensional ising model as a soluble problem of many fermions. *Rev. Mod. Phys.*, 36:856–871, Jul 1964.

[70] Andrew W. Senior, Richard Evans, John Jumper, James Kirkpatrick, Laurent Sifre, Tim Green, Chongli Qin, Augustin Žídek, Alexander W. R. Nelson, Alex Bridgland, Hugo Penedones, Stig Petersen, Karen Simonyan, Steve Crossan, Pushmeet Kohli, David T. Jones, David Silver, Koray Kavukcuoglu, and Demis Hassabis. Improved protein structure prediction using potentials from deep learning. *Nature*, 577(7792):706–710, 2020.

[71] Huitao Shen, Bo Zhen, and Liang Fu. Topological band theory for non-hermitian hamiltonians. *Phys. Rev. Lett.*, 120:146402, Apr 2018.

[72] David Sherrington and Scott Kirkpatrick. Solvable model of a spin-glass. *Phys. Rev. Lett.*, 35:1792–1796, Dec 1975.

[73] Anton Souslov, Benjamin C. van Zuiden, Denis Bartolo, and Vincenzo Vitelli. Topological sound in active-liquid metamaterials. *Nature Physics*, 13(11):1091–1094, 2017.

[74] Howard Stone. *Lecture notes of MAE552 (Spring 2020)*. 2020.

[75] W. P. Su, J. R. Schrieffer, and A. J. Heeger. Solitons in polyacetylene. *Phys. Rev. Lett.*, 42:1698–1701, Jun 1979.

[76] Joseph A. Sulpizio, Lior Ella, Asaf Rozen, John Birkbeck, David J. Perello, Debarghya Dutta, Moshe Ben-Shalom, Takashi Taniguchi, Kenji Watanabe, Tobias Holder, Raquel Queiroz,

Alessandro Principi, Ady Stern, Thomas Scaffidi, Andre K. Geim, and Shahal Ilani. Visualizing poiseuille flow of hydrodynamic electrons. *Nature*, 576(7785):75–79, 2019.

[77] D. J. Thouless, M. Kohmoto, M. P. Nightingale, and M. den Nijs. Quantized hall conductance in a two-dimensional periodic potential. *Phys. Rev. Lett.*, 49:405–408, Aug 1982.

[78] John Toner and Yuhai Tu. Flocks, herds, and schools: A quantitative theory of flocking. *Phys. Rev. E*, 58:4828–4858, Oct 1998.

[79] D. C. Tsui, H. L. Stormer, and A. C. Gossard. Two-dimensional magnetotransport in the extreme quantum limit. *Phys. Rev. Lett.*, 48:1559–1562, May 1982.

[80] Tamás Vicsek, András Czirók, Eshel Ben-Jacob, Inon Cohen, and Ofer Shochet. Novel type of phase transition in a system of self-driven particles. *Phys. Rev. Lett.*, 75:1226–1229, Aug 1995.

[81] Sagar Vijay, Jeongwan Haah, and Liang Fu. A new kind of topological quantum order: A dimensional hierarchy of quasiparticles built from stationary excitations. *Phys. Rev. B*, 92:235136, Dec 2015.

[82] X. G. Wen. Chiral luttinger liquid and the edge excitations in the fractional quantum hall states. *Phys. Rev. B*, 41:12838–12844, Jun 1990.

[83] B. Widom and J. S. Rowlinson. New model for the study of liquid–vapor phase transitions. *The Journal of Chemical Physics*, 52(4):1670–1684, 1970.

[84] C. N. Yang. The spontaneous magnetization of a two-dimensional ising model. *Phys. Rev.*, 85:808–816, Mar 1952.

[85] C. N. Yang and T. D. Lee. Statistical theory of equations of state and phase transitions. i. theory of condensation. *Phys. Rev.*, 87:404–409, Aug 1952.

[86] Shunyu Yao and Zhong Wang. Edge states and topological invariants of non-hermitian systems. *Phys. Rev. Lett.*, 121:086803, Aug 2018.

[87] Kazuki Yokomizo and Shuichi Murakami. Non-bloch band theory of non-hermitian systems. *Phys. Rev. Lett.*, 123:066404, Aug 2019.

[88] Junyi Zhang. Artificial gauge fields and spin-orbit couplings in cold atom systems. *arXiv:1312.7486*, 2013.

[89] Junyi Zhang. Dipolar dimer liquid. *arXiv:1902.08890 [cond-mat.stat-mech]*, 2019.

[90] Junyi Zhang, Jérôme Beugnon, and Sylvain Nascimbene. Creating fractional quantum hall states with atomic clusters using light-assisted insertion of angular momentum. *Phys. Rev. A*, 94:043610, Oct 2016.

[91] Linfeng Zhang, Jiequn Han, Han Wang, Roberto Car, and Weinan E. Deep potential molecular dynamics: A scalable model with the accuracy of quantum mechanics. *Phys. Rev. Lett.*, 120:143001, Apr 2018.

[92] D Zhou, D. Z. Rocklin, M. Leamy, and Y. Yao. Topological invariant and anomalous edge states of fully nonlinear systems. *arXiv:2012.14103*, 2020.

[93] Di Zhou and Junyi Zhang. Non-hermitian topological metamaterials with odd elasticity. *Phys. Rev. Research*, 2:023173, May 2020.

[94] Di Zhou, Leyou Zhang, and Xiaoming Mao. Topological edge floppy modes in disordered fiber networks. *Phys. Rev. Lett.*, 120:068003, Feb 2018.

[95] Di Zhou, Leyou Zhang, and Xiaoming Mao. Topological boundary floppy modes in quasicrystals. *Phys. Rev. X*, 9:021054, Jun 2019.